N O T I C E

THIS DOCUMENT HAS BEEN REPRODUCED FROM
MICROFICHE. ALTHOUGH IT IS RECOGNIZED THAT
CERTAIN PORTIONS ARE ILLEGIBLE, IT IS BEING RELEASED
IN THE INTEREST OF MAKING AVAILABLE AS MUCH
INFORMATION AS POSSIBLE

Final Report

to

THE NATIONAL AERONAUTICS AND SPACE ADMINISTRATION

for

NASA Contract NAS 9-15582

SPACE ENVIRONMENT AND LUNAR SURFACE PROCESSES

Principal Investigator: Dr. George M. Comstock

COSMOSCIENCE ASSOCIATES, INC.

21 Erland Road, Stony Brook, N.Y. 11790

September 25, 1979

Introduction.

This Report describes work done on the Space Environment and Lunar Surface Processes project by Dr. George M. Comstock under NASA Contract NAS 9-15582 initiated March 15, 1978.

Our primary accomplishment under this contract has been the development of a general rock/soil model capable of simulating in a self-consistent manner the mechanical and exposure history of an assemblage of solid and loose material from submicron to planetary size scales, applicable to lunar and other space-exposed planetary surfaces. The model has been incorporated into a new computer code called MESS.2 (Model for the Evolution of Space-exposed Surfaces.) MESS.2 represents a considerable increase in sophistication and scope over previous soil and rock surface models, as described in this Report. CosmoScience Associates Technical Report TR-104 describing the MESS.2 model structure and operation and reprints of papers published under Contract NAS 9-15582 are attached as part of this Report.

MESS.2 is currently being applied under NASA Contract NASW 3273 to continue our study of planetary surface development and space environment characteristics.

General Rock/Soil Model.

It has been one of our long-range goals to develop a modeling technique for the multi-scale problem of space-exposed surfaces which would be detailed, self consistent, and generally applicable to a wide variety of planetary surface conditions,

both rock and soil, in order to put the interpretation of measured exposure
and maturation indices on a firmer theoretical basis. We believe that
MESS.2 will go a long way toward achieving this goal. The model is actually
a system of programs that allow the problem to be broken down into tractable
parts, or scale regimes, with a consistent set of assumptions, while main-
taining accurately the interactions among different regimes. Within each
scale regime the surface and event characteristics, initial conditions, and
program bookkeeping can be flexibly tailored to suit the physical processes
important on that scale. Details of MESS.2 are discussed in the attached
summary; improvements made over the last year are described below.

Our previous models for soil (Comstock, 1977, 1978--attached) and for
rock (Comstock, 1978--attached) were designed to study specific problems.
The soil model (called RHOSOL) demonstrated the relations among various
track density and density gradient statistics as a function of physical
near-surface exposure parameters; and the rock model (MESS.1) demonstrated
the effect on track profiles of erosion scale and intermittent dust shielding.
These models also served as useful prototypes for new modeling techniques
and demonstrated the value of this approach, although as we pointed out in
our 1978 Progress Report, they were too limited in scope for many applications.

With this earlier work as a basis, considerable testing and background
work has been applied over the last year to increase the usefulness of the
model results.

Table 1 compares some of the capabilities of our previous models for
near-surface soil and dusty rock surfaces with the current general rock/soil
model MESS.2. All models treat individual cratering events chosen randomly
from a size-frequency distribution of impact events and record residence

depths on a continuous depth scale. Important improvements are summarized below.

Soil Model Upgraded--MESS.2 allows for the first time our full multi-scale "bootstrap" technique to be applied to soil simulation, as we have done for rock surfaces. This is important for modeling the intercorrelation of maturation and mixing of soil over different depth and area scales, and hence for studying the theoretical relation of soil statistics, evolutionary paths, time variations, and core chronology. MESS.2 follows the lateral movement of soil and provides areal correlations of soil atatistics, which was not possible with our previous soil model. In addition MESS.2 tailors crater shape and ejecta districtuion to local topography and slope for both soil and rock surfaces.

Layered Medium--A basic improvement in MESS.2 is the capability of handling a general layered medium where the layers may have different strengths, such as loose material on a solid surface. Different crater morphologies are used for each layer where appropriate. The model generates composite (e.g. bench) craters when the top layer is breached. All surface statistics (exposure time, erosion accreta, etc.) are recorded for the upper surface of each layer. The current application of this capability is to a more detailed and complete study of the properties and effects of loose grains and bonded accreta on rock surfaces. There are also larger-scale applications, for example to shallow regoliths and small bodies, which we will investigate.

Individual Particles--A very important new feature of MESS.2 is the ability to follow an ensemble of individual loose particles of the appropriate size range. These "particles" may be fine accreta, soil grains, fragments,

rocks, or boulders depending on the scale size regime. When exposed, the particles are subjected to finer-scale processes (impacts, accretion) and their exposure times are recorded. Other statistics such as track and pit densities also can be recorded for individual particles. Our previous soil model followed only one grain at a time, so no correlation among local grain histories was possible. MESS.2 includes these correlations which are important for studying the properties of in situ reworking vs. mixing over larger depths and distances. These considerations are vital, for example in isolating the effects of time variations in meteoroid and nuclear particle fluxes from statistical fluctuations in exposure history.

This individual grain capability is equally important for rock surfaces where an accurate derivation of surface exposure time distributions in the presence of bonded accreta and loose dust depends on the distribution of single- and few-grain layers. On a larger scale this capability allows a derivation of the expected distribution and residence times of ejected rocks. This would have implications for dating craters and would set constraints on the time variation of galactic cosmic rays used to determine rock residence times and on the rate of impact events governing rock residence.

The cratering process is well understood when the crater size is either much larger or much smaller than the particle size being impacted. The treatment of individual grains allows us to better handle the difficult intermediate case where crater size is less than about an order of magnitude larger than the typical loose particle size, so that relatively few grains are involved. This is a critical range important for thin layers (miniregoliths) on both rock and soil surfaces where maturation processes predominatly operate.

Consequently we have attempted in MESS.2 to pay careful attention to the fate of individual grains on sub-centimeter size scales.

New Ejecta Model—During the last year we have developed for MESS.2 a new ejecta origin and distribution model which allows exposure depth histories, lateral movement, and the effect of local topography to be simulated more accurately. The model uses an ejecta distribution map given, on a horizontal surface, by the form:

$$r_a = (Q+1)R_c - QR_c[(h/fH_c) + (r/R_c)^2]^\alpha$$

where r_a is the final radial distance of the ejecta, R_c is the apparent crater rim radius, $H_c = 0.4R_c$ is the maximum depth of the final crater in loose material, Q, f, and α are shape parameters, and h and r are the pre-ejection depth and radial distance, respectively, within the crater. This map assumes that the ejecta origin contour surfaces for r_a within the crater are paraboloids with respect to a horizontal surface. α controls the radial dispersion of ejecta, f controls the shape of the rim (takes account of fallback) and Q controls the maximum ejecta range for "normal" ejecta (not high velocity).

We find that a good set of parameters is Q=10, f=1.2, and α =0.2. These values produce an ejecta blanket, shown in Figure 6 of the attached MESS.2 summary, which has a realistic rim shape and a height distribution proportional to $(r_a/R_c)^{-3}$ (compare with McGetchin et al., 1973). This also produces an ejecta origin map, shown in Figure 5 of the attached summary, similar to experimental results (e.g., Piekutowski, 1975). The model yields stratigraphy inversion and stretching similar to that observed (e.g., Stöffler et al., 1975); it is also similar to the model proposed by Croft (1977) except that our form produces a more realistic ejecta origin

map and explicitly includes the final rim shape.

Surface slope and curvature can be taken into account by assuming a similar relation for ejection angle:

$$\theta_a = \theta_x - (\theta_x - \theta_m)[(h/fH_c) + (r/R_c)^2]^\beta$$

where $\theta_x \cong 90^\circ$, $\theta_m \cong 10^\circ$, and $\beta \cong \alpha$, and translating .. a new ballistic range assuming the same ejection velocity.

We believe the new ejecta model can be applied to a wide range of size scales, although this "normal" ejecta becomes much less important in the total cratering energy budget for smaller craters, where a very small fraction of ejected mass apparently carries off most of the kinetic energy at high velocities (e.g., Breslau, 1970).

MESS.2 applies this ideal model for each event to the actual distribution of particles and soil and rock surface topography as described in the attached summary. This ejecta model will have an important application in asteroid regolith studies.

Agglutination and Comminution--MESS.2 incorporates a tentative, first-approximation model for generating bonded accreta (e.g., "pancakes") and agglutinates and keeps account of these. The material ejected from the central pit of rock microcraters is identified with strongly bonded accreta. Material ejected from a similar central region of small soil craters is only partially melted and is assumed to form into agglutinates. MESS.2 assumes that individual particles are broken up when they receive an impact that would yield a crater of similar diameter.

Track Densities--The distribution of track densities is maintained both in soil grains and in rock profiles as in our earlier models.

Statistical Scale Coupling--The statistical techniques for coupling finer-scale activity into the simulation of a given scale regime have been

improved and made more detailed. The previous rock and soil models assumed constant, average rates for accretion and erosion, which could not yield detailed surface exposure distributions. Between discrete events in a given size regime, MESS.2 chooses the finer-scale erosion or accretion for each cell from a set of model-generated time-dependent depth-frequency distributions appropriate to the environment at that cell (e.g., bare rock or particle, or fine material). See the discussion and Figure 14 in the attached summary. In each of these distributions a given depth change has associated exposure statistics so that an accurate average exposure time at the surface of each cell is maintained, including the effects of finer-scale activity.

Multi-scale Correlations--The areal and frequency distributions of surface features (e.g., microcraters, accreta, solar wind concentrations) can be generated a d correlated as a function of time on any size scale by using the exposure time distributions derived on that scale and the time-dependent areal and frequency distributions derived for that feature on its appropriate scale. These distributions can also be correlated against track densities and profiles. These theoretical correlations between processes operating on different scales, under various surface and flux level conditions, are the results needed to help interpret rock and soil measurements.

Current Applications--We consider the MESS.2 system to be a general research tool which has many applications. It is currently being applied to study rock surface processes in greater detail. We are in the process of generating the time-dependent areal and frequency distribution functions for exposure time and other statistics as discussed in the previous sections, over the submicron to centimeter size scales. Theoretical correlations

between microcrater and accreta densities and track profiles are among the results to be obtained from these. We are seeking improved criteria for locating production track profiles, determining micrometeoroid and solar wind fluxes and exposure times, and identifying past variations in these fluxes.

We also are applying the model to the maturation of lunar soil, to derive theoretical correlations among maturation indices, identify the effect of evolutionary paths--in situ reworking vs. mixing of pre-irradiated soil--and to improve criteria for determing soil core chronology and soil sources. The goal is to put many of the interpretations of soil measurements on a sounder theoretical basis.

References

Breslau D. (1970) Partitioning of energy in hypervelocity impact against loose sand targets. J. Geophys. R s. 75, 3987-3999.

Comstock G. M. (1977) On deciphering the particle track record of lunar regolith history. J. Geophys. Res. 82, 357-367.

Comstock G. M. (1978) Miniregoliths I: Dusty lunar rocks and lunar soil layers. Proc. Lunar Planet. Sci. Conf. 9th, p. 2557-2577.

Croft S. K. (1977) Energies of formation for ejecta blankets of giant impacts. In Impact and Explosion Cratering, Roddy, Pepin, and Merrill (eds.), Pergamon Press, p. 1279-1296.

McGetchin T.R., Settle M., and Head J.W. (1973) Radial thickness variation in impact crater ejecta: Implications for lunar basin deposits. Earth Planet. Sci. Lett., 20, 226-236.

Piekutowski A. J. (1975) The effect of variations in test media density on crater dimensions and ejecta distribution. Air Force Weapons Laboratory, Kirtland Air Force Base, New Mexico, AFWL-TR-74-326.

Stöffler D., Gault D. E., Wedekind J., and Polkowski G. (1975) Experimental hypervelocity impact into quartz sand: Distribution and shock metamorphosis of ejecta. J. Geophys. Res. 80, 4062-4077.

TABLE 1. MODEL FEATURES

Model Feature	RHOSOL (soil) 1977,78	MESS.1 (dusty rock) 1978	MESS.2 (rock/soil) 1979
Random, discrete impact events........	yes	yes	yes
Continuous depth scale recorded.......	yes	yes	yes
Multi-scale iteration technique.......	partly (single scale with finer-scale accretion)	yes	yes
Surface distribution recorded.........	no	yes	yes
Topology-dependent crater and ejecta morphology.....................	no	partly (crater)	yes
Layered medium capability.............	no	partly (dust thickness)	yes
Ensemble of individual grains.........	partly (single grain)	no	yes
Ejecta origin and range monitored.....	no	no	yes
Generation of bonding accreta and agglutinates included.............	no	no	yes
Comminution included..................	no	no	yes
Distribution of track densities.......	yes	yes	yes
Time-dependent areal and frequency distributions and correlations of exposure times and of erosion and accretion depths......................	no	partly (averages used to couple scales)	yes

MODEL FOR THE EVOLUTION OF SPACE-EXPOSED SURFACES

I: Summary of MESS.2 Structure and Operation

George M. Comstock

July 31, 1979

SUMMARY OF MESS.2 STRUCTURE AND OPERATION

Structure--Space-exposed surfaces are good examples of a type of environment governed by processes, such as meteoroid impacts, which operate over a wide range of size and time scales, producing complex inter-scale relationships between observable quantities. One general method of attacking this type of multi-scale problem is to solve or model it for a restricted range of size and/or time scales,parameterize the results in a form that has meaning on the next larger scale, and reiterate the procedure on the larger scale.

MESS.2 is a system of programs that uses this approach to analyze the evolution of space-exposed surfaces, although the basic structure has applications to other multi-scale problems. Figure 1 summarizes the roles played by the various programs in the system. Each program acts as a utility routine to perform certain bookkeeping or physical simulation functions on separate files that contain data on the surface and frequency distributions of statistics, statistics for individual grains, and depth profiles. Furthermore each of these can be tailored for each size scale to suit the physical processes important on that scale. The whole system can run automatically or parts can be used individually to study the effect of each model process. Some of the essential model features are described below.

Surface grid and size scale--For each size scale regime simulations are carried out on a surface grid made up of hexagonal cells, illustrated in Figure 2. Each cell has an effective radius S such that πS^2 is the area of one cell. S defines the scale or resolution of the size regime. The location of a cell is identified by a special near-circular coordinate system composed of hexagonal "rings" denoted by N, where N=0 is the central

cell, and an angular cell count M which ranges from M=1 to M=6N for ring N. The hexagonal symmetry allows the grid to be divided into 6 sectors, each containing N cells from each ring N. A grid of N rings contains 1+3N(N+1) cells, or 2791 cells for N=30, a convenient recorded grid size.

Individual events are chosen centered on a random cell and each event is analyzed in a similar event-centered coordinate system (n,m). This allows convenient handling of circularly symmetric cratering characteristics as well as sectoring of the event to handle asymmetries, for example in topography. Simple conversion algorithms relate (N,M) and (n,m). A special algorithm can correct for the non-circularity of the rings but does not change the results significantly and is generally not worth the extra computation time. It is found to be sufficient to treat each ring as representing an average radial distance, which encloses the same area, given by:

(1) $R = (1+3N^2)^{1/2} S \cong \sqrt{3} \ NS$

Crater surface statistics are recorded for each cell. These include elevation, exposure age, number of times excavated, and a surface condition code describing the last event to affect the cell. The condition code is used on output to help identify surface features generated, such as craters and bonded accreta.

Depth scale--Elevations at each cell are recorded on a continuous scale, allowing fractions of S, and represent an average over the cell area. Depth profiles (for example, track density) are monitored at a set of sample points defined on a logarithmic depth scale. If the surface erodes then the logarithmic depth scale is maintained by generating new sample points by logarithmic interpolation between existing sample points. Depth profiles are recorded only at certain cells, especially the central cell. Excavated sample points are retained along with excavation time and depth as well as initial depth.

Time scale--For each size regime the model time scale is based on the mean time T between individual impact events. Individual events occur at time intervals t chosen from the distribution exp(-t/T) and constrained to be multiples of a model time step dT=T/10. The use of a fixed model time step is necessary to handle continuous events--track accumulation and smaller-scale activity. The distributions used to simulate smaller-scale activity are generated from smaller-scale simulations at time intervals of dT so that one will match the event interval t. The exposure time for each cell may actually contain a fraction of dT because smaller-scale activity affects the average exposure time for each cell. Statistical distributions are updated and permanently stored at specified time intervals and read out either later or at specified intervals.

Event sizes--The range of event sizes that are treated individually in a given size regime is chosen to maintain good resolution for the smallest craters, which are generally the most abundant as well. The largest crater considered, generally rare on the regime's time scale, is always smaller than the smallest crater on the next larger size regime in the multi-scale iteration sequence. Figure 3 shows three typical rock microcraters with central pits and spall zones; n is a crater index referring to the number of rings in the central pit. n=1 is the smallest crater considered and n=11 is the largest when size regimes vary by a factor of 10 in scale size S. The crater index is also referred to in this summary as N_p.

Within this size range every impact event is treated individually if it excavates material from within the recorded grid even if its center lies outside. Larger craters therefore can have a larger "impact parameter" so an appropriately weighted size-frequency distribution is used to determine T and choose event sizes. Typical size-frequency distributions are dis- cussed by Comstock (1978--attached). Ejecta material deposited from more

distant events with craters completely outside the recorded grid is treated as part of "continuous activity". This is found to be a good approximation that saves considerable time.

Layered medium--Either one or two surfaces may be defined--a top surface and, optionally, a sub-surface which may have different characteristics. All surface statistics are followed for both surfaces. Both surfaces together define a distinct top layer over deeper material, for example a surface soil layer over older soil, soil over rock, or weak rock over stronger rock. The last two cases involve different cratering characteristics for each layer, which often results in composite craters. The potential exists for defining additional layers.

For the case of thin soil on rock surfaces Figure 4 shows to scale a progression of nominal crater shapes as a function of soil thickness H. Pure soil and rock microcraters are shown at top and bottom, respectively. Corresponding soil and rock craters are related by the relation:

$$(2) \qquad R_c = R_s (\rho_r / \rho_c)^{1/3}$$

where ρ_r and ρ_c are rock and soil density, respectively, and

$$(3) \qquad R_s = 4R_p = 4 \sqrt{3} \; N_p S$$

where N_p is the crater index. For microcraters MESS.2 forms composite crater shapes by simple superposition of pure shapes.

Individual particles--Individual particles are defined in a particle list which records the elevation of the particle center and other individual particle attributes. These may include surface exposure time, track density, pit density, and other statistics of interest. Each cell in the surface grid has a pointer giving the position in the particle list of the topmost particle at the cell. Each particle in the list has a pointer giving the position in the list of the next particle down at that cell. Pointers and elevations are reassigned as particles are excavated and redeposited.

Individual particles and soil matrix material ejected from the recorded grid area are generally returned to the grid either by individual events centered outside or by more distant "continuous" activity. However it is possible to define an exterior (larger-scale) slope for each sector which controls the efficiency of this external contribution and determines the amount of ejecta thrown back. This can result in either net erosion or net accretion for the recorded surface. Any extra particles needed for this are copied at random from those in the particle list. This procedure allows rock and summit erosion and crater fill-in to be simulated.

Normally particles are initially defined only for loose material between the top surface and the sub-surface discussed above. New particles are generated when the sub-surface is excavated and are given attributes consistent with recorded sub-surface statistics and profiles.

Ejecta mapping--Material is ejected by an impact event according to the model relation:

$$(4) \qquad r_a = (Q+1)R_c - QR_c \, [(h/fH_c) + (r/R_c)^2]^{\alpha}$$

where R_c is the crater radius, H_c is central depth, shape parameters are given the values $Q=10$, $f=1.2$, and $\alpha =0.2$ for lunar soil, r is initial radial distance from impact point, h is initial depth below the local mean plane surface (defined below), and r_a is the nominal emplacement distance from impact on a horizontal surface.

On sloping surfaces or small bodies the actual ejecta distance can be found by further assuming an ejection angle given by:

$$(5) \qquad \theta_a = \theta_x - (\theta_x - \theta_m)[(h/fH_c) + (r/R_c)^2]^{\beta}$$

where we use $\theta_x = 80^{\circ}$, $\theta_m = 10^{\circ}$, and $\beta = \alpha$. θ_a is measured with respect to the local surface which may itself have a slope angle of θ_s. The corrected ejecta distance r_s can be found for any size body by using the spherical ballistic equation and assuming the same ejection velocity V:

(6) $\quad v^2 = R_a g_a/(\cos^2 \theta_a + \sin 2\theta_a/2\tan[(r_a-r)/2R_a])$

$\quad = R_s g_s/(\cos^2(\theta_a + \theta_s) + \sin 2(\theta_a + \theta_s)/2\tan[(r_s-r)/2R_s]).$

In this relation R_s, g_s, R_a, and g_a are the planetary radius and gravity

of the actual body and of the model reference body (the Moon), respectively.

For $g_s = g_a$ and $R_s = R_a \gg r_a$ Equation 6 reduces to:

(7) $\quad r_s = r + (r_a-r) \sin2(\theta_a + \theta_s)/\sin2\theta_a$

The actual ejecta distance can be finally adjusted for the surface elevation

near r_s (farther downslope, nearer upslope) by taking $\theta_a + \theta_s$ as the incident

angle and searching along it from r_s to find the surface. General downslope

movement will result from this process.

For soil the final crater shape is assumed to be parabolic with $H_c = 0.4 R_c$.

For rock microcraters a more complex pit and spall zone is used as shown in

Figure 3, with spall zone omitted for pits less than about 10 microns diameter

(see Comstock, 1978--attached).

The origin map of ejecta distances given by Equation 4 for a lunar

regolith crater on a horizontal surface is shown in Figure 5. The corres-

ponding radial dependence of the ejecta blanket height is shown in Figure 6.

For subcentimeter craters formed in soil the movement of individual particles--

grains and fragments--becomes important. Individual particles are considered

to be ejected when their centers are above the nominal crater bottom. The

depth of the particle center also determines the final distance of the

ejected particle.

Figures 7, 8, and 9 illustrate this for the idealized case of a flat

surface with neatly packed particles all of radius S (the cell radius).

Figure 7 shows ejecta origin maps for the two smallest crater sizes, with

crater indices $N_p = 1$ and 2. Each box represents one ejected grain; for

100-micron diameter grains these represent craters of radii about 0.5 mm and

1.0 mm. The dotted lines are the nominal crater shapes, N is the initial

event-centered ring number, and the number in each box is the final ring number of the ejected particle. Figures 8 and 9 show the resulting ejecta patterns of the grains (dots) for N_p = 1 and 2 craters, respectively. Crater contours in units of 2S are also shown. The six "rays" are artifacts of the grid geometry but they do mimic observed ray patterns. Figure 10 shows the result of a typical sequence A to D of five such events generated randomly for a recorded grid of 30 rings. Event C has N_p = 2 and the others have N_p = 1; event D is centered just outside the grid. In this case all grains ejected from the grid have been thrown back in between events by "continuous" activity exterior to the grid, as is appropriate for an infinite horizontal surface where matter is conserved. Note the superposition of events.

Event procedure--During a typical simulation individual events will be more complicated than those described above because the surface will not be smooth and level, both loose and hard surfaces may be involved, and the loose surface layer may include matrix material as well as individual particles. The following event procedure is used:

1) The event location (cell L_e) and size (crater index N_p) are chosen at random as described earlier.

2) In event-centered coordinates, the crater is divided into 7 regions, a central region of N_p rings and 6 sector portions extending from N_p to N_c (corresponding to crater radius R_c) as shown schematically in Figure 11. The average surface elevation <E> in each region is determined and a local slope for each sector, σ_i = tan θ_s, is determined from $<E>_i$ - $<E>_c$ such that volume under the sector surface is conserved.

3) The elevation of nominal rock and soil crater bottoms is determined in each sector relative to the local slope. A typical example is shown in Figure 12 for a thin soil cover over rock. The soil in Figure 12 contains

both individual particles and matrix material but the particles are not shown, for clarity.

4) The actual composite crater bottom is determined from rock and individual particle elevations.

5) Starting at the rim and working inward, and from surface down, to assure proper stratigraphy inversion, material is taken out of the crater and re-deposited at its ejecta distance, as described above, using its initial height relative to the local slope.

6) Soil material taken from the central region is re-assigned as agglutinitic fragments (partly melted, loosely bonded). Rock material from the central region forms agglutinitic material if it lands on soil, bonded accreta if it lands on bare rock. (These are first approximations subject to improvement.)

Between individual events the next event time interval is chosen and smaller-scale and other "continuous" activity is processed over that interval. Continuous activity includes ejecta throwback, subject to any external slope as discussed earlier, and track accumulation in individual particles and in rock profiles. At the end of the interval statistics may be compiled, saved, and read out as needed. The next individual event is then processed.

Statistics and multi-scale coupling--Periodically, surface, particle, and profile statistics are compiled and saved. To analyze activity on a given size regime, distributions of exposure time, erosion and accretion rates, number of impacts, etc. are compiled for both surfaces over most of the recorded grid (a few rings near the rim are ignored to reduce edge effects). To properly couple different size regimes, these statistics are also compiled over "supercells" similar in area to the unit cell area of the next larger-scale regime.

Figure 13 illustrates the procedure. Regimes I, II, and III represent

successively larger size scales, in this case a factor of ten each step

or x100 in area. Suppose Regime II is currently being simulated. Statistics

for Regime II are averaged within each supercell outlined (5 rings, 91 cells

each) and the averages are formed into a distribution of supercell statistics,

along with the results of other trial runs if needed to form significantly

detailed distributions. As explained in the section on time scales, these

distributions are formed at time intervals most useful to the next larger-

scale Regime III. Similarly distributions formed when Regime I was simulated

are used by Regime II to simulate "continuous" smaller-scale activity.

Correlations between supercells are ignored but this is a good approximation.

Two basic statistics are essential to couple two regimes--a depth

change and an average exposure time. Other smaller-scale statistics can

be correlated with these on their appropriate scale to form over-all distri-

butions and correlations between scales. Figure 14 shows schematically the

types of depth change distributions that are generated for a given size

regime as a function of time and three general environments--eroding, stable,

and accreting. Each distribution has exposure time parameters correlated

with it (not shown).

A typical surface may shift locally from one condition to another so

the distributions tend to broaden. During the crater production phase much

of the surface is unaffected or only accreting lightly. These earlier phases

are generally the most important for micro-scale regimes because of the

meteoroid distribution knee at about 50 microns crater diameter (Comstock,

1978-- attached). Larger-scale regimes (e.g., whole rocks, craters filling and

eroding, rille edges eroding, etc.) need to be followed into the crater

saturation region for complete characterization.

For the particular time interval t between two events, the appropriate

distribution is applied to each cell to choose at random the smaller-scale

activity at that cell. The depth change chosen has associated with it two parameters governing exposure time: the fraction F of area affected by events during the appropriate time interval t and the average $<t_a>$ exposure time for that fraction. These, together with the previous average exposure time $<T_a>$ at the cell, are used to calculate the new average exposure time $<T_a>'$ at that cell, just before the next event, according to the relation:

$$(8) \qquad <T_a>' = (1-F)(<T_a> + t) + F<t_a>$$

In this way the average exposure time for each cell is maintained with a minimum of error compounding between size regimes.

Smaller-scale accreta is treated as matrix material. If the diameter of an individual particle is reduced by 20% or more by smaller-scale erosion then it is considered crushed and the remainder is re-assigned as matrix material.

Depth profile development--Between events track densities are updated for particles and depth profiles taking into account true (density reduced) shielding depth below an average local exposure surface determined separately for each sector. Depth profiles are maintained on a logarithmic scale as described earlier. An example of profiles for bare rock generated as a function of time is shown in Figure 15. Four sample points are illustrated at a, b, c, and d. After production for (in this case) 4600 years profile A is attained. Excavation at this time of a 230 micron chip (including point a) results very briefly in profile B. After an additional 4700 years profile C is attained, nearly regaining the production slope. Excavation of 74 microns at this time gives profile D, with point b ejected. An additional 110,000 years without further excavation yields profile E.

Track production profiles typically used are discussed by Comstock (1978--attached). Production profiles for other processes may be similarly incorporated into the model.

Applicability--MESS.2 is designed to be very flexible in executing, monitoring, and permanently storing simulation results so that they may be put to the greatest use. The model system is designed as a research tool that can be tailored to many applications of space-exposed surface conditions. The structure of the system and many of its initialization, monitoring, and output routines are general enough to be used for other simulation problems. MESS.2 is currently being applied to rock surface and soil development problems and the results will be presented in future CosmoScience Associates Technical Reports.

Reference:

Comstock, G. M. (1978) Miniregoliths I: Dusty lunar rocks and lunar soil layers. Proc. Lunar Planet. Sci. Conf. 9th, p.2557-2577.

Figure Captions

Fig. 1.   Major programs in MESS.2 system and their function.

Fig. 2.   MESS.2 coordinate system showing ring number N and
angular cell count M.

Fig. 3.   Typical model crater shapes for microcraters in rock
or glass surfaces; n=1 is the smallest crater used.
Stippled area is the central pit.

Fig. 4.   Series of model microcrater shapes in layered medium
ranging from thick soil cover to bare rock.

Fig. 5.   Model ejecta origin map for a soil crater. Ejecta
distance is r_a, initial distance and depth are r and
h, respectively. H_c and R_c are crater depth and
apparent radius, respectively.

Fig. 6.   Model height distribution for a continuous ejecta
blanket; h_a is height, r_a is distance from impact.

Fig. 7.   Model ejecta origin maps for craters excavating two
and three layers of individual soil grains.

Fig. 8.   Final distribution of grains ejected from top crater
in Figure 7.

Fig. 9. Final distribution of grains ejected from bottom crater in Figure 8.

Fig. 10. Distribution of grains resulting from a typical sequence of events similar to those in Figures 7-9. Events occuring outside of the grid area shown are taken into account.

Fig. 11. Sectoring of an impact event to determine local slopes from average elevations <E> in each sector.

Fig. 12. Cross section of typical model impact event in complex soil-covered rock surface indicating construction of final composite crater.

Fig. 13. Schematic representation of statistically coupling different size regimes by averaging results over supercells similar in area to individual cells on the larger size scale.

Fig. 14. Schematic representation of typical depth change distributions as a function of time for different surface conditions.

Fig. 15. Example of a typical development with time (A to E) of track density depth profiles in bare rock, involving two impact excavations at profile site. The evolutionary paths followed by four individual rock crystals (a-d) are shown; a and b are excavated.

OUTLINE OF MESS.2 STRUCTURE

Initialization Package

M E S R U N   Defines basic model parameters

M E S B L D   Initializes adjustable "Run" parameters (scale
                     size, production rates, surface characteristics)
                     and builds various utility tables

M E S M O D   Defines characteristics of individual events
                     (nominal crater shapes and ejecta maps)

M E S R E C   Defines characteristics of "continuous" activity
                     (tailors distributions simulating finer-scale
                     activity and defines depth profile formats)

Run Package

M E S I N T   Initializes data files (resets surface) for new
                     "trial", or picks up where previous trial left off

M E S T R L   Controls simulation trial sequence and times

M E S C O N   Processes continuous activity between individual
                     events

M E S U P D   Generates statistical distributions as needed

M E S O U T   Reads out statistical frequency distributions as
                     needed

M E S S E E   Reads out surface distributions as needed

M E S C A T   Processes individual events

FIGURE 1

Figure 2

Figure 3

Figure 4
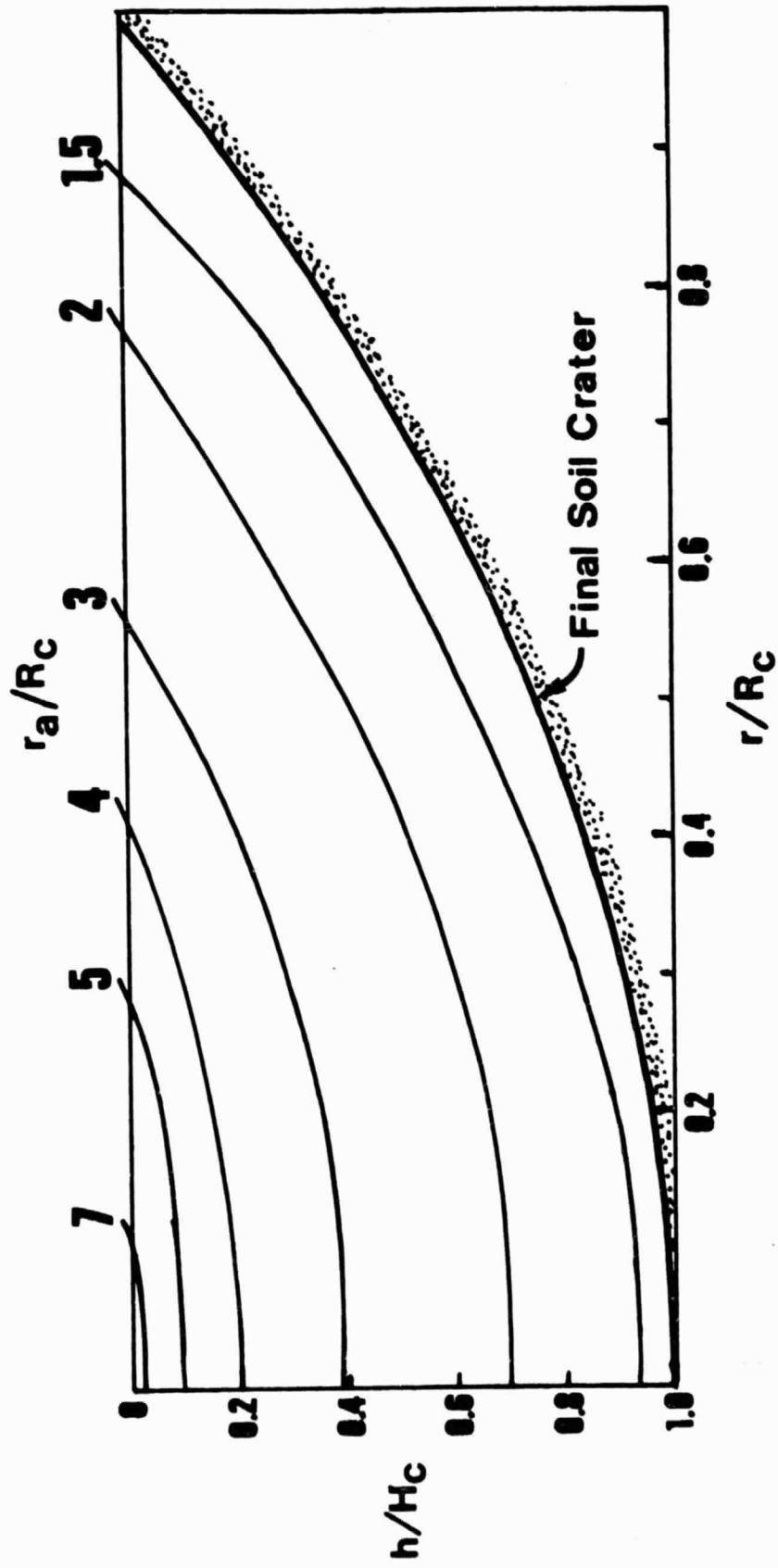
Final Soil Crater

Figure 5

Figure 6

$N_P=1$

$N_P=2$

Figure 7

$N_P=1$

Figure 8

N_P-2

Figure 9
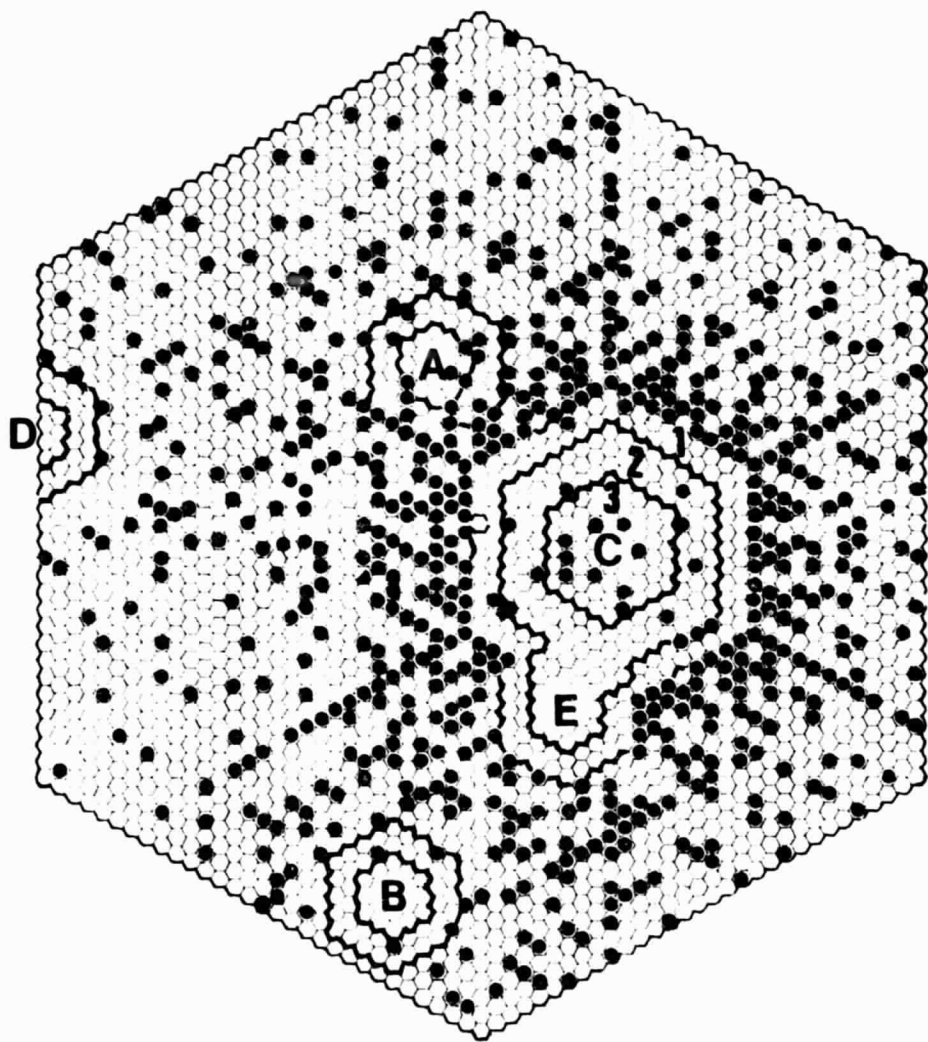
Figure 10

Figure 11

Figure 12

Legend:
- Initial Soil Surface
- Initial Rock Surface
- Average Local Surface
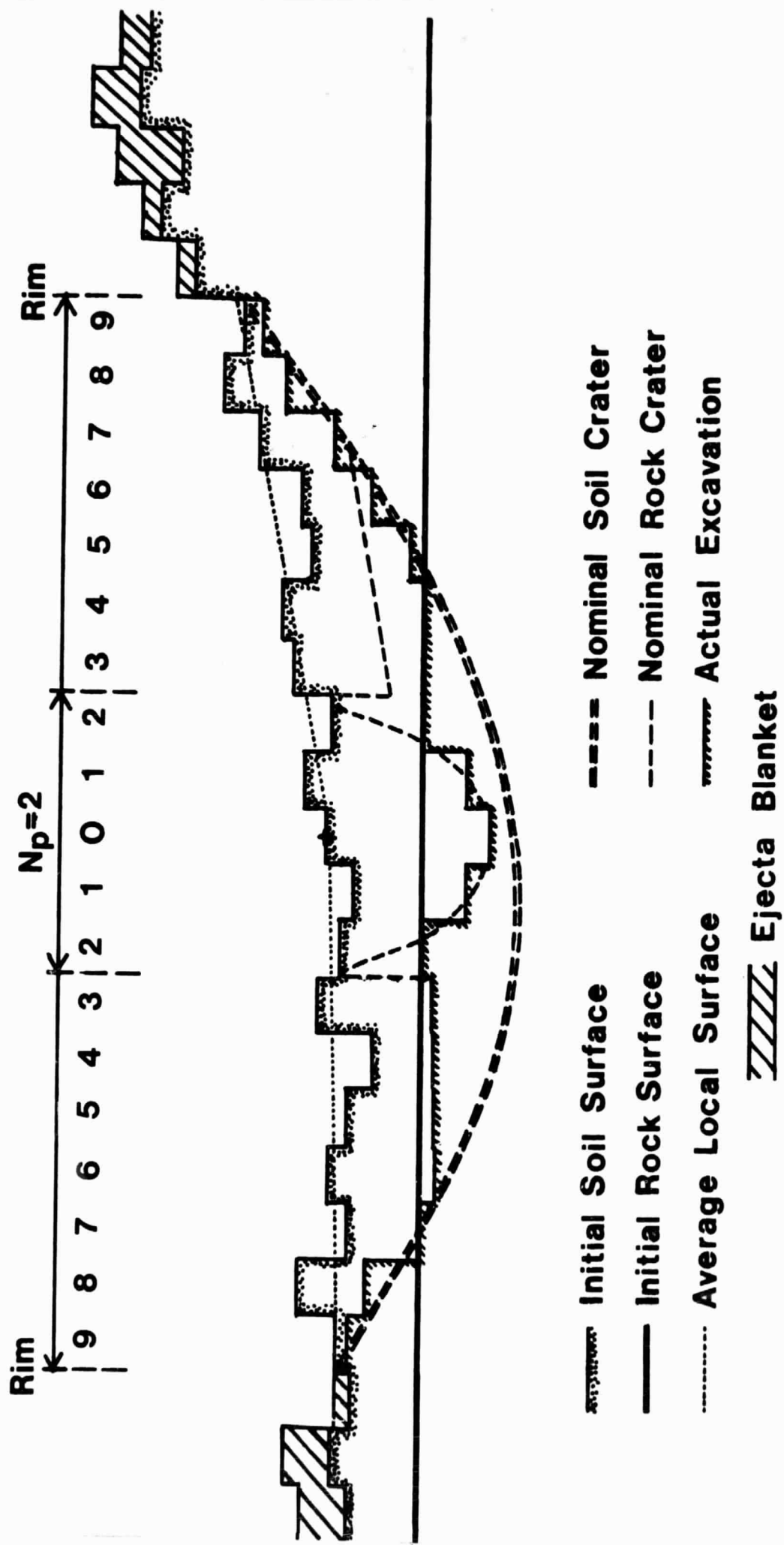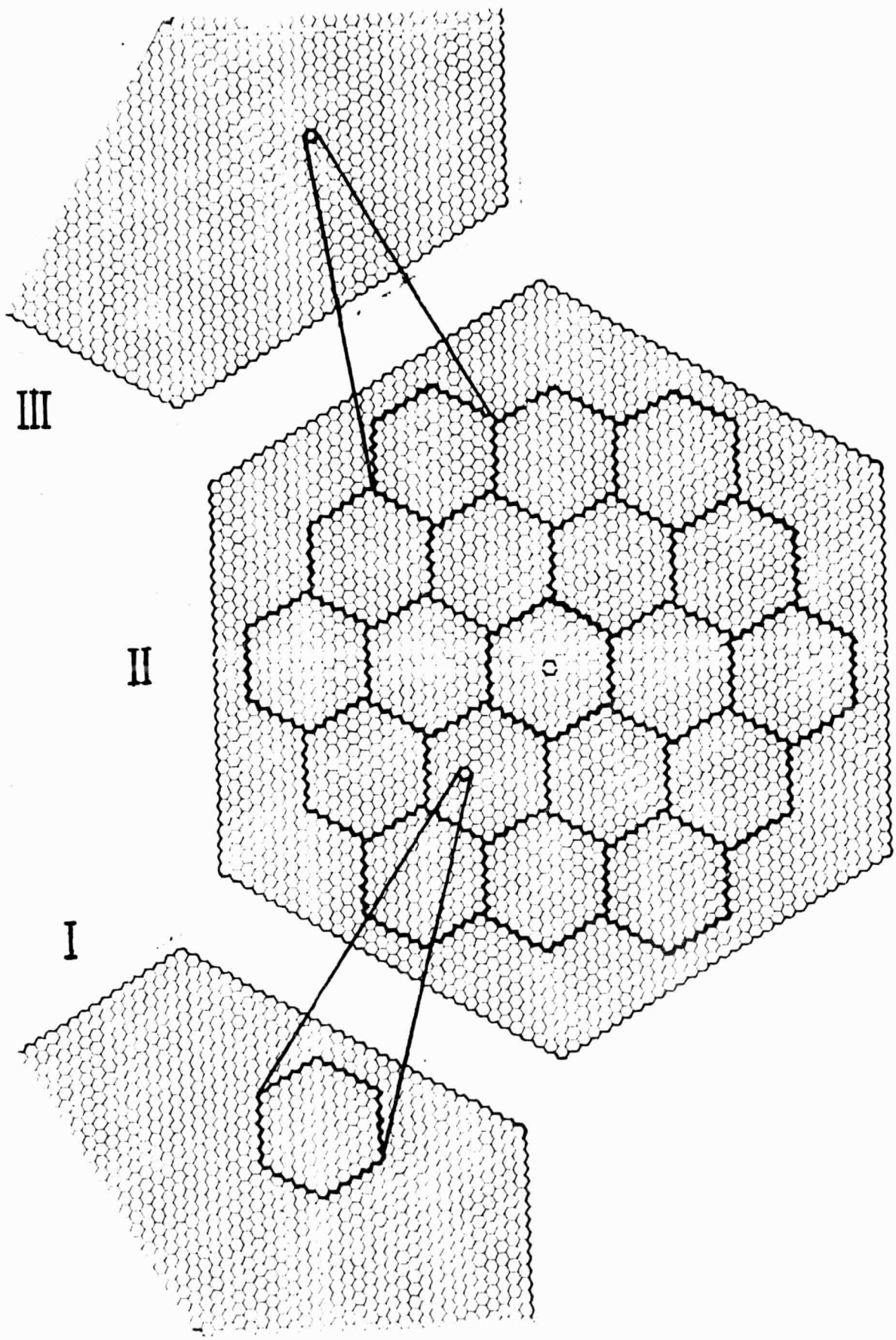- Nominal Soil Crater
- Nominal Rock Crater
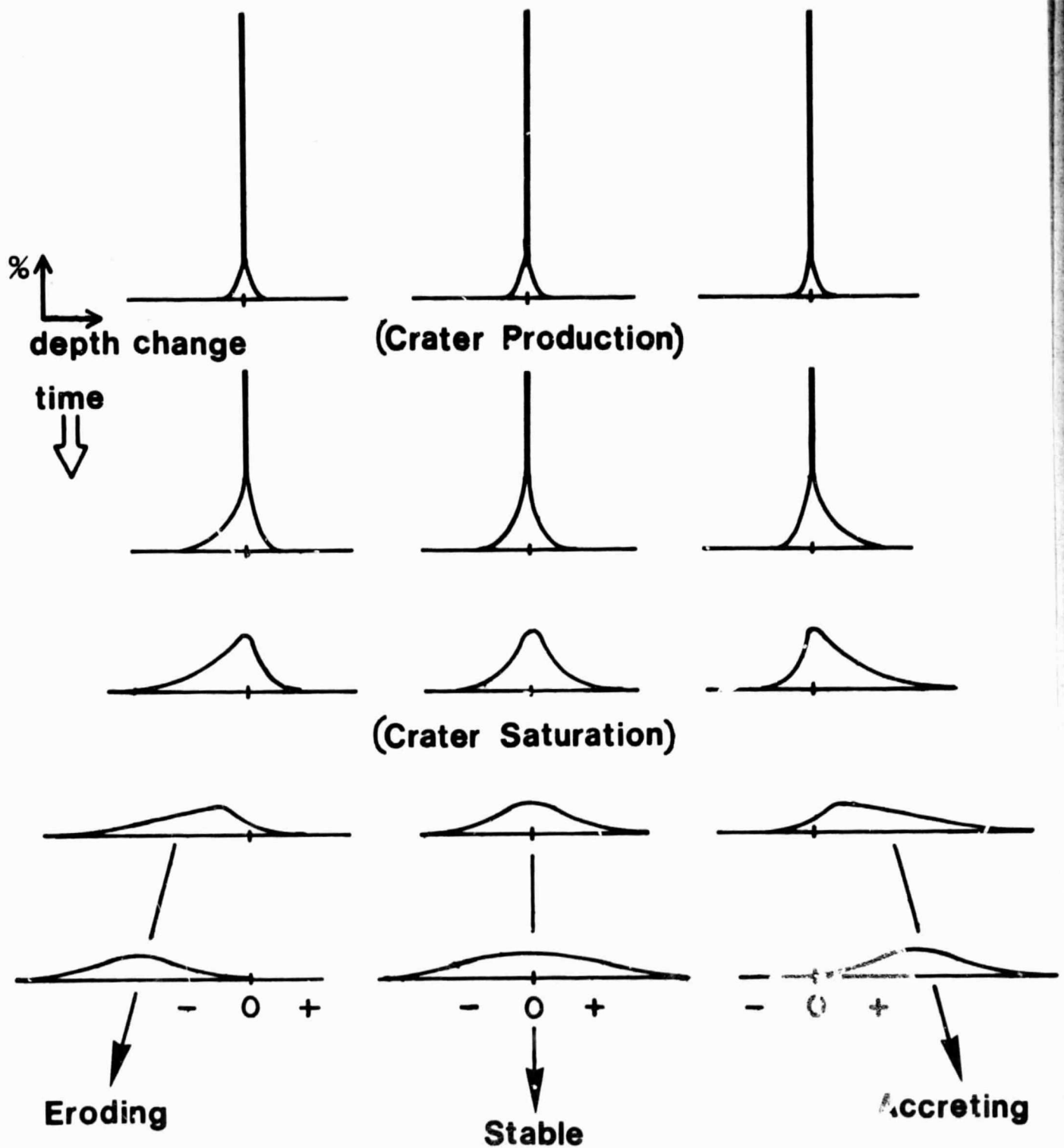- Actual Excavation
- Ejecta Blanket
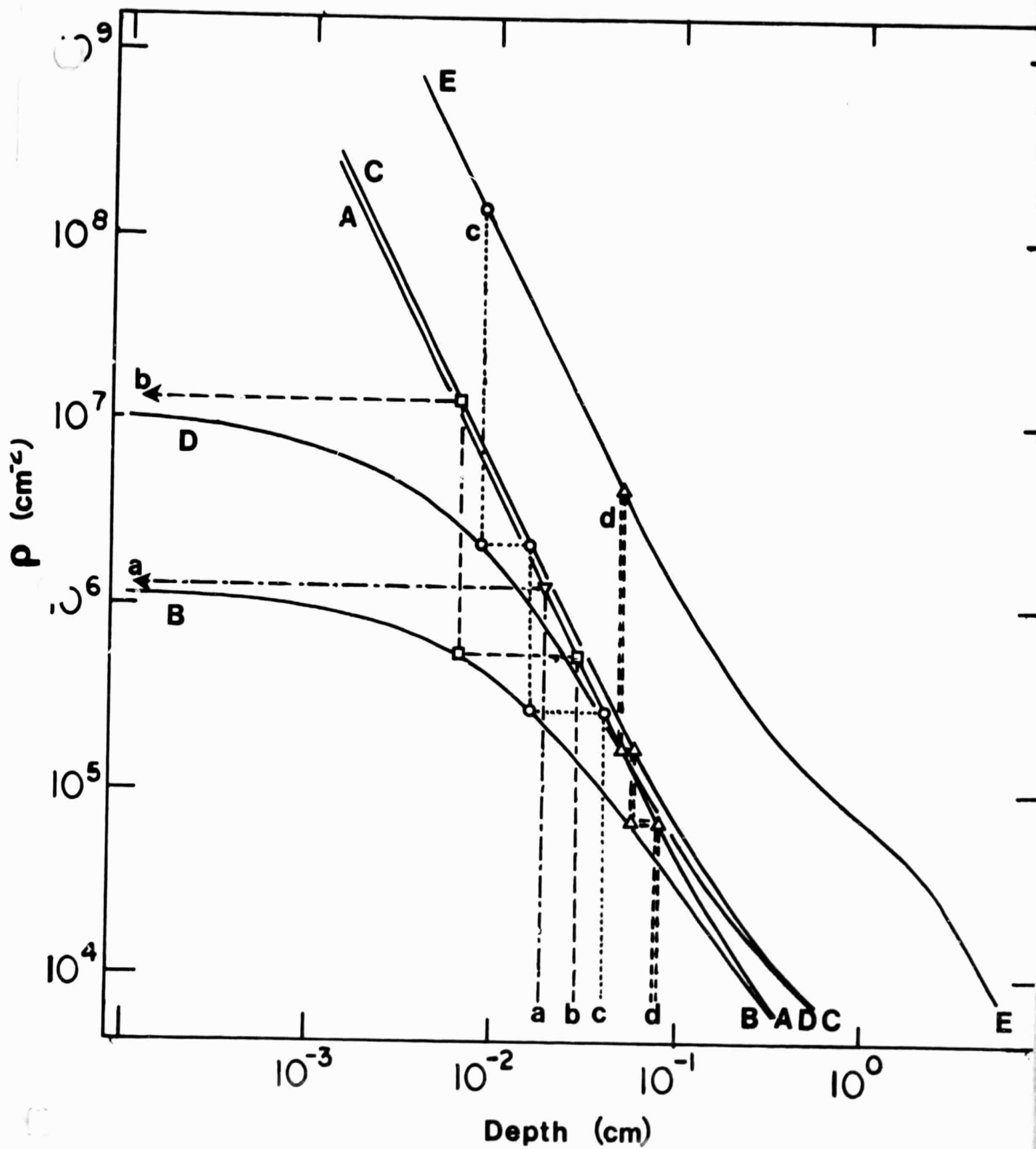
III

II

I
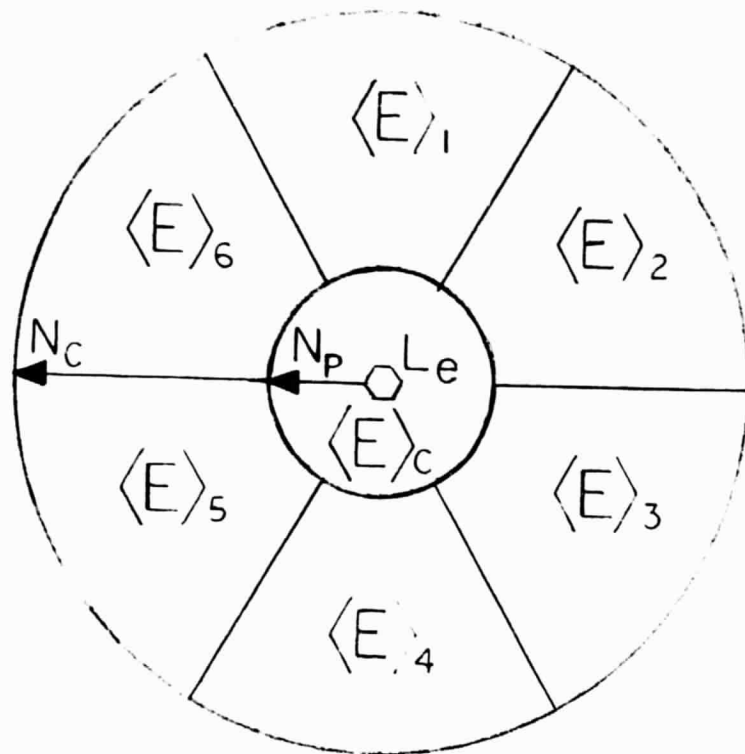
Figure 14

Figure 15

MINIREGOLITHS AND MONTE-CARLO MODELING
George M. Comstock, CosmoScience Associates,
21 Erland Road, Stony Brook, New York   11790

Modeling Methods--During this first decade of close-hand observation of lunar materials it has become apparent that one of the most striking characteristics of the lunar surface environment is the great range of time and size scales over which surface processes have been occurring. Most importantly, the size distribution of meteoroid impact events is such that properties of material at any given site can be influenced by impacts of any size scale, from accumulated microscopic events to single Imbrium-scale events. These properties are governed by processes that are important on time scales ranging from very short-lived (individual impacts, large solar flares) to geologic (accumulated effects of many impacts, of solar wind and flare activity and cosmic ray irradiation, geologic processes, etc.)

Since physical and chemical processes on each size and time scale are modulated by mechanical processes operating on a wide range of scales, there will be a complex feedback among various scales of activity and complex, variable correlations among the observable quantities (e.g., maturation indices, pit densities, track parameters, gas content, stratigraphic profiles, etc.) Because of this feedback between scales of activity and the statistical nature of impact events, it is very difficult, if not impossible, to obtain a complete understanding of lunar rock and regolith properties by analytic methods alone or by brute-force simulation of all scales at once, with details severely truncated by computer limitations. These difficulties have been discussed before (1-3).

This complexity can be made tractable by recognizing that a series of events which are distinguishable, catastrophic occurrences on one time scale will appear as a gradual change over a longer time scale, and a collection of objects which have a discrete extent on one size scale can be represented as a continuous medium on a larger size scale. We can then generalize to a bootstrap modeling technique whereby a given scale of activity is simulated by considering individual catastrophic events and discrete objects distinguishable on that scale and by treating all shorter time scale events as gradual, continuous changes and smaller size scale objects as an evolving continuous matrix. The properties of these continuous features are governed by statistical distributions derived by simulations on smaller activity scales. In the other direction, larger scale events and objects determine the general environment for a particular activity and hence their effect can be included in terms of local parameters or boundary conditions. These parameters are not arbitrary or fixed but reflect statistical properties of larger scale activity.

This modeling technique is very efficient, self-consistent, and demonstrates with good resolution the effects of each process as a function of scale. After calibration against lunar

MINIREGOLITHS AND MODELING

Comstock, G. M.

measurements the results can be used to model any space-exposed
surface. By adjusting the processes involved the technique
is applicable to the special surface-atmosphere-space interface
problems represented by various planetary surfaces. Like other
aspects of lunar research this approach is presenting insights
into terrestrial problems as well.

Miniregoliths--We have been developing this approach in an
extensive computer program called MESS (Model for the Evolution
of Space-exposed Surfaces). A simplified version of
MESS was used to simulate the erosion of lunar rocks and to
demonstrate the effect of intermittent dust coverings on the
evolving track density profiles in rocks (3,4). An earlier,
prototype model for soil has already provided new relationships
between track parameters and near surface soil history (2,4).
MESS may be applied to any scale of activity, however the larger
size scales have been more extensively modeled (e.g., 1, 5-8)
so we concentrate initially on sub-cm scales where many critical
surface processes occur and new data are becoming available
(e.g., 9-11).
To emphasize this we introduced last year (4) the general
concept of the "miniregolith", a sub-cm regime of loose material
either actively covering rocks, asteroid surfaces, or soil or
else buried in fossilized soil layers. MESS is currently being
applied to two miniregolith problems: exposure limitations by
dust on rocks and the maturation of soil by sub-cm processes.
For dusty rocks we derive model surface exposure time distribu-
tions in the presence of dust and seek to establish model
relationships among, for example, the densities of solar wind
implanted gases, submicron pits, accreta, larger microcraters,
and particle tracks. For soil our goal is to derive relation-
ships among the various maturation parameters under various
surface conditions, in order to improve criteria for character-
izing ancient soil surfaces and soil mixtures and to allow us
to extract more information from the vast amount of lunar soil
data already available. Our results so far are closely related
to the concept of two evolutionary paths suggested by McKay et
al. (12).
The full version of MESS represents an integrated rock/soil
model which treats individual particles (grains, fragments,
rocks) as well as craters on a given scale. For miniregoliths
a particle size distribution and graininess of the soil are
taken into account. In this way we can include the crushing,
aggregation, and lateral and vertical movement of individual
particles, while keeping account of their orientation, surface
exposure, pit densities, and track densities. The behavior and
evolution of micron- to millimeter-sized particles can be
followed.
The cratering process is well understood when the crater
size is either much larger or much smaller than the particle
size being impacted. One of the main modeling difficulties
arises when the impact crater size is less than on order of

MINIREGOLITHS AND MODELING

Comstock, G. M.

magnetude larger than the typical loose particle size, so that relatively few particles are involved. Most of these will be ejected or shifted, some will be vaporized, melted, crushed, or fractured, and some will be compressed and aggregated with impact melt, or accrete to particle, rock, or glass surfaces. This is often the case for dusty rock surfaces and surface soil layers, with grain sizes on the order of 1 micron to 100 microns and dominate crater diameters on the order of 10 microns to 1mm. There is evidence that high velocity secondaries may also be important (13). The MESS format is capable of taking these processes into account to the extent that they are understood on the scale involved and prove to be significant. Ultimately this program will find application to the evolution of space-exposed surfaces at all stages of development, from bare rock, to rubble, to fresh soil, to mature regolith.

References:
1. Gault D. E., Horz F., Brownlee D. E., and Hartung J. B. (1974) Proc. Lunar Sci. Conf. 5th, p. 2365-2386.
2. Comstock G. M. (1977) J. Geophys. Res. 82, 357-367.
3. Comstock G. M. (1977) In Lunar Science VIII, p. 202-204.
4. Comstock G. M. (1978) Proc. Lunar Planet. Sci. Conf. 9th, (in press). (Abstracts in Lunar and Planetary Science IX, P. 189-191, 192-194.)
5. Arnold J. (1975) Proc. Lunar Sci. Conf. 6th, p. 2375-2395.
6. Duraud J. P., Langevin Y., Maurette M., Comstock G. M., and Burlingame A. L. (1975) Proc. Lunar Sci. Conf. 6th, p. 2397-2415.
7. Horz F., Schneider E., and Hill R. E. (1974) Proc. Lunar Sci. Conf. 5th, p. 2397-2412.
8. Oberbeck V. R., Quaide W. L., Mahan M., and Paulson J. (1973) Icarus, 19, 87-107.
9. McDonnell J. A. M. (1977) Proc. Lunar Sci. Conf. 8th, p. 3835-3857.
10. Morrison D. and Zinner E. (1977) In Lunar Science VIII, p.691-693.
11. Zook H., Hartung J. B., and Hauser E. (1978) In Lunar and Planetary Science IX, p.1300-1302.
12 McKay D. S., Fruland R. M., Heiken G. H. (1974) Proc. Lunar Sci. Conf. 5th, p. 887-906.
13 Flavill R. P., Allison R. J., and McDonnell J. A. M. (1978) In Lunar and Planetary Science IX, p. 323-324.

Miniregoliths I: Dusty lunar rocks and lunar soil layers

G. M. COMSTOCK

CosmoScience Associates
21 Erland Road, Stony Brook, New York 11790

Abstract—Using a detailed Monte-Carlo model for rock surface evolution we have verified that erosion processes alone cannot account for the shapes of the solar flare particle track profiles generally observed at depths of about 100 μm and less in rocks. We demonstrate that the observed profiles are easily explained by a steady accumulation of fine dust at a rate of 0.3 to 3 mm/10^6 years, depending on the micrometeoroid impact rate which controls the dust cover and results in maximum dust thicknesses on the order of 100 μm to 1 mm.

We have derived the commonly used lunar soil track parameters (ρ_{min}, ρ_q, ρ_{med}, N_H/N) in terms of parameters characterizing the exposure of soil grains in the few-millimeter-thick surface mixing and maturation zone which is one form of miniregolith. We present ρ_q vs. ρ_{min} and N_H/N vs. ρ_q plots which allow us to determine the degree of mixing in soil samples and the amount of processing (maturation) in surface miniregoliths. The ratio ρ_q/ρ_{min} is particularly sensitive to the mixing of soils of different maturities and we use it to show that the sampling process often artificially mixes together finer distinct layers, and that ancient miniregolith layers on the order of a millimeter thick are probably common in the lunar soil.

1. INTRODUCTION

The history of exposure of material on any space-exposed surface determines the extent of and correlation among many maturation processes, such as microcrater formation, accreta collection, solar wind implantation and chemical alterations, solar flare particle track accumulation, and glassy agglutinate formation in soil. The details on this exposure history are governed primarily by impact events that affect material within the first few millimeters of the surface (Gault *et al.*, 1974 for soil; Hörz *et al.*, 1974 for rock) and possibly by other surface transport processes such as electrostatic effects (Criswell, 1972; Pelizzari and Criswell, 1978.) We may define, therefore, a zone of a few millimeters thick at space-exposed surfaces in which maturation actively takes place. Except for rock surfaces constantly kept clean, this maturing zone will involve a layer of loose, impacted material which we call a miniregolith. As part of a general study of such miniregoliths we have been investigating the two types of space-exposed lunar surfaces, rocks and soil, using Monte-Carlo calculations together with primary particle track data.

In the case of rock surfaces we seek in this paper to establish the general existence of thin, variable dust coatings. The possibility of occasional loose dust on rocks has usually been accepted, but not studied systematically. The term dust refers to rather fine-grained material that has been kicked, blown, levitated, or

otherwise transported from one surface to another and settles loosely or sticks to the surface.

The generally pitted and rounded aspect of rock surfaces exposed on the order of a million years or more indicates that over a long time mass wastage by primary impacts dominates the rock surface morphology on a scale of greater than about a millimeter. Comparison of the density of etchable tracks left by galactic cosmic ray iron nuclei with the concentration of cosmogenic nuclides produced by cosmic ray protons yields an upper limit of 0.5–2 mm/10^6 years for the mass wastage rate (Crozaz et al., 1974.)

Surface exposure history on a scale less than about 1 mm can be studied using the depth profiles of solar flare particle track density. Some examples of depth profiles in rocks and a review of the mechanisms involved can be found in Fleischer et al. (1975). These profiles generally show an inverse power law exponent of about 1 to within 10 μm of the present surface, and have been explained as representing an equilibrium between rock erosion and track production (e.g., Crozaz et al., 1971.) However, such shallow equilibrium profiles can be maintained down to 10 μm or less only if the erosion mechanism removes chips on a very fine size scale of less than about 10 μm. Moreover, the track density attained by the equilibrium profile depends on the rate of this erosion and measured profiles imply about 0.2–0.8 mm/10^6 years (see review by Fleischer et al., 1975.)

A difficulty arises when we look for an erosion mechanism acting on a scale of 10 μm or less with this high rate. We will show in the next section that erosion by micrometeoroid impacts alone cannot account for the observed track profiles at depths ≤ 100 μm; it generally removes chips that are too large. Atomic sputtering (e.g., McDonnell et al., 1972; McDonnell and Carey, 1975), thermal flaking (Seitz and Wittels, 1971), and other fine-scale mechanisms are at least two orders of magnitude too weak. Moreover, we find no direct evidence in the form of gradual degradation of microcraters for any fine-scale surface erosion of the required rate. These considerations force us to investigate other mechanisms which affect the surface exposure history.

Fine-scale erosion is not the only mechanism which will produce the observed solar flare track profiles. Any process which leads to a distribution of exposure depths roughly uniform on a scale of about 10 μm increments will have the same effect. The most likely such process would be a continual accumulation of small dust grains (note that a single "slab" layer will not work). We know that dust generated by relatively distant events is continually falling on the soil surrounding the rock. It is reasonable to assume that some of it will stick to the rock, however loosely, especially the smaller size fraction. This accumulation of dust would be modified and occasionally knocked off by micrometeoroid impacts and possibly by elecrostatic effects. A fraction of this accreta sticks well enough to be observed after sampling and cleaning (McDonnell, 1977; Zook et al., 1978.)

We have modeled these processes with a Monte-Carlo computer program called MESS (Model for the Evolution of Space-exposed Surfaces) and report the first results in this paper. We shall show that for reasonable values of dust

accumulation rates and micrometeoroid fluxes we can reproduce the observed solar flare particle track profiles and densities and account for a wide variation from rock to rock while maintaining intermittent, variable dust coatings of ~100 μm to ~1 mm thickness.

In the case of lunar soil, previous model calculations (e.g., Gault *et al.*, 1974; Duraud *et al.*, 1975; Comstock, 1977a) have included a surface mixing zone, or lunar skin, but this has not been related in a generally useful way to the various statistical track parameters (e.g., minimum, quartile, and median track densities) often used to characterize the measurements in individual soil layers (see, for example, Crozaz *et al.*, 1970; Arrhenius *et al.*, 1971; Bhandari *et al.*, 1973; Fleischer *et al.*, 1974; Crozaz and Dust, 1977; and others.) Price *et al.* (1975) and Goswami *et al.* (1976a) have used track parameters to identify microstratigraphy in impregnated core tubes, which could represent ancient surface maturation zones or miniregoliths. In the third part of this paper we derive typical track parameters in terms of model parameters governing surface exposure. The results allow us to establish quantitative criteria for determining the degree of mixing in individual soil samples and the amount of processing through surface miniregoliths. The evidence suggests that ancient miniregolith layers are common in the lunar soil.

2. How Dusty are Lunar Rocks? Evidence from Track Profiles

Rock model

The rock surface calculations in this paper were made using a new Monte-Carlo computer model which we have developed to serve as a general vehicle for the simulation of surface-correlated processes in any size range. The model uses a bootstrap technique which quickly generates an impacted surface of any desired scale and resolution while faithfully simulating topography and the distribution over the surface of exposure ages and erosion rates, explicitly giving the size-scale dependence of each. This model was first reported by Comstock (1977b).

Our method is to divide the crater population into consecutive size regimes; in the present case we use a factor of 10 in pit diameters: 0.4–4 μm, 4–40 μm, 40–400 μm, and so on. Starting with the smallest physically significant regime, the model is run for each regime long enough to establish the effects of discrete events in that size regime, that is until an equilibrium surface is well established. Each such run tells us how the distribution of surface exposure times, surface erosion, number of surviving craters, and so on develop with time for that regime. At each step the erosion in. nation can be used as input for the next larger regime in order to establish cumulative effects as follows. There is some variable interval of time between simulated events for a given size regime. During that time interval the cumulative effects of smaller-scale regimes are included by assigning to each cell a depth change, or no change, dependent on that time

interval and chosen from the distribution of erosion depths found by earlier runs for smaller-scale regimes.

Clearly this procedure can be extended to any size scale without either consuming computer time, needlessly processing the much more numerous smaller events, or ignoring them altogether. The time thus saved can be used to compute other information, such as track accumulation. The limited size range of each regime allows us to reduce the number of cells and to set a uniformly high resolution; in each regime the smallest event considered can cover many cells; 91 in the present model. The total simulated surface area thus scales with the size regime. This bootstrap procedure has an advantage over previous rock surface calculations (Hartung *et al.*, 1973; Hörz *et al.*, 1974) which require the processing of a great many small events before the effects of large events become statistically meaningful. Time limitations then prevent larger events from being considered and computer size limitations prevent much small-scale resolution. Hörz *et al.* (1974) use a cell size of 400 μm square; our smallest cell size used is 0.2 μm diameter and smaller size ranges could easily be considered.

We employ the nominal crater shape shown in Fig. 1 which has a central pit (stippled) and spall zone (shaded). For a pit diameter D_p, the pit depth $H_p = 2D_p/3$, the spall zone diameter $D_s = 4D_p$ at the original surface sloping down to $3D_p$ at the bottom, which has a depth $H_s = 0.4D_p$. The pit is formed by a spherical bottom tangent to a cone with opening angle $\theta_O = 40°$. This shape is based on observed microcraters (Hörz *et al.*, 1974, 1975; Brownlee *et al.*, 1975). Although the central pit generally represents a small fraction of the microcrater volume, we define it carefully because the model records which cells represent pit glass. In this way surviving microcraters may be identified by the same criterion as is used experimentally, that is preservation of the central pit (Hartung *et al.*, 1973; Hartung *et al.*, 1975). This idealized crater shape is translated to the quantized surface grid in such a way as to preserve volume, as shown in Fig. 2 for the smallest event ($n = 1$), the largest event ($n = 11$), and an intermediate size ($n = 6$).

Other innovations are included in the model which we believe enhance its faithfulness is simulating rock surface processes. We use a hexagonal close-packed grid of cells, not the usual rectangular grid. A hexagonal grid possesses
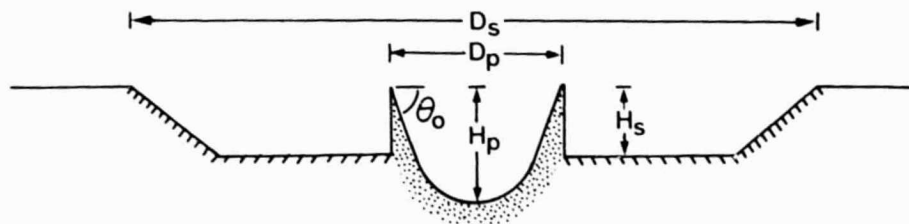

Fig. 1. Idealized cross-sectional shape of microcraters used in rock surface model. Stippled area is glassy pit, shaded area is spall zone which tends to be absent for D_p less than ~10 μm.

the unique property that it has nearly circular symmetry, at least locally, about any cell in the grid (and the noncircularity is easily corrected). This is very efficient for reproducing the circular symmetries inherent in impact events. It also conveniently enables us to divide the spall zone of each event into six independent angular sectors each of which we allow to conform to the average radial slope of the pre-spall surface in that sector while removing local high spots. The result is more convincing topography and reliable results. Studies of microcraters have shown (Hörz et al., 1975) that pits of diameter on the order of 10 μm or less tend to lack spall zones, which decreases their erosion efficiency. In the model all pits of less than 4 μm diameter have no spall zones, all pits of greater than 40 μm have normal spall zones, and between 4 μm and 40 μm pits have a probability ranging from 0 to 1, respectively, of having a spall zone in a given angular sector.

Some impact pit production rates used with the model are shown in Fig. 3. The distribution marked *lunar rock data* is essentially the same curve preferred by Hörz et al. (1974), extended to smaller pit diameters based on the measurements of Morrison and Zinner (1977); we use an analytic form given by: $N(>D) = 8.3 \times 10^{-7}D^{-3} + 8.3 \times 10^{-4}(D + 0.005)^{-3}$ where D is the pit diameter in cm and N is the cumulative crater production rate per $cm^2 - 10^6$ years. Some satellite measurements are indicated by solid points for comparison; see Hörz et al. (1975) for a complete discussion of satellite measurements and a compilation of references.
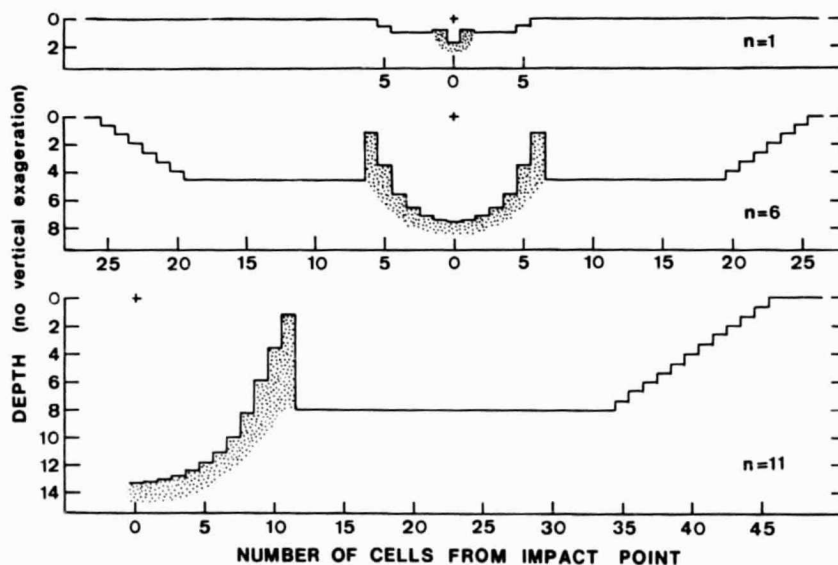

Fig. 2. Examples of microcrater shapes on actual rock model grid. Within a given size-scale regime, $n = 1$ is the smallest crater considered and $n = 11$ is the largest, with 11 size steps altogether. The $n = 1$ crater has an area of 91 cells on the hexagonal grid used.
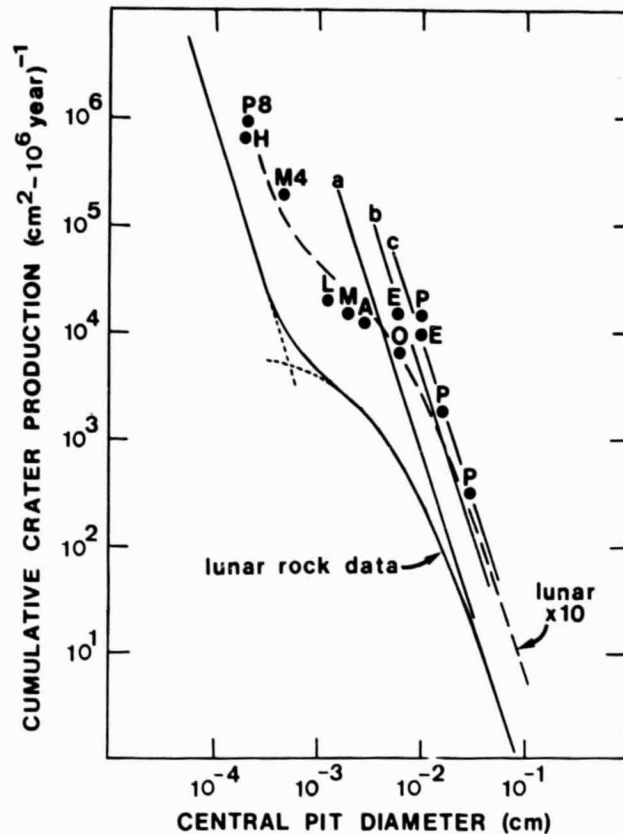
G. M. COMSTOCK

Fig. 3. Cumulative microcrater production curves used in rock surface model. Curve marked *lunar rock data* is from Hörz *et al.* (1974) and Morrison and Zinner (1977). Solid points are satellite measurements: A—Apollo windows; E—Explorer XVI and XXIII; H—HEOS 2; L—Lunar Explorer 35; M—Mariner II; M4—Mariner IV; O—Lunar Orbiter 1–5; P—Pegasus I, II, III; P8—Pioneer 8 (see Hörz *et al.*, 1975).

The model accumulates track densities at sample points assigned on a logarithmic depth scale; if these sample points are eroded away during the course of a simulation run, the computer generates new points by interpolation to maintain the logarithmic grid. In this way the track density profile is accumulated efficiently over a wide depth range. Some track production profiles that have been suggested are shown in Fig. 4 for a semi-infinite medium. Curves a, b, and d are for solar flare particles, curve c is due to galactic cosmic rays.

Track profile data

A large number of particle track density vs. depth profiles have been measured in lunar rocks by several groups since the first samples were returned. In order to
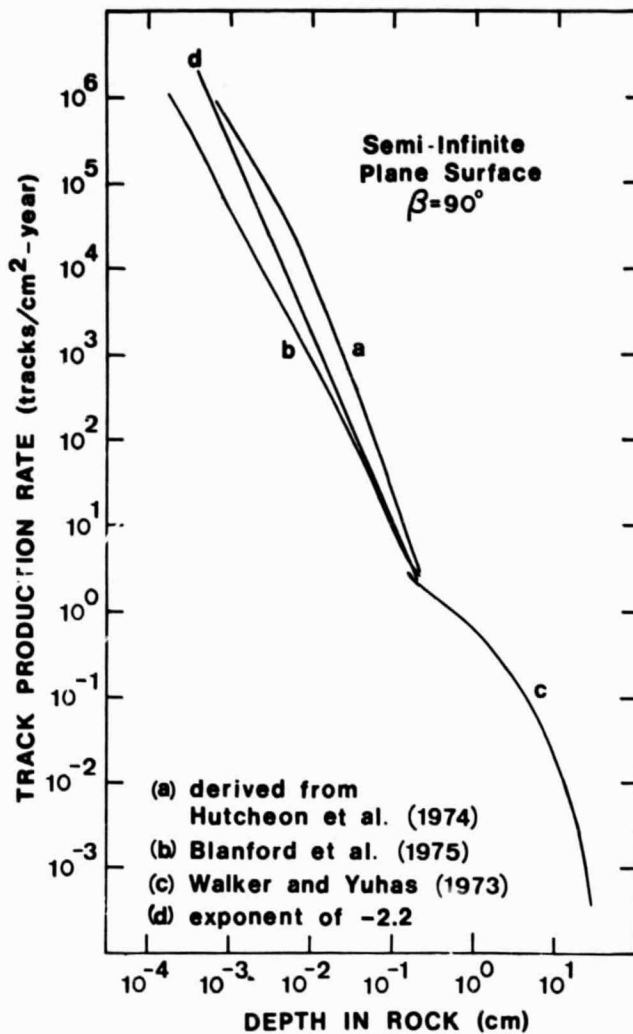
Fig. 4. Iron-group track production rates suggested by lunar samples carefully chosen to reduce the complicating effects of erosion and dust. All of these rates were tried in the rock surface model.

present clearly the relevant features of these data we have plotted in Fig. 5 the track density at a depth of 100 μm vs. the negative exponent (log-log slope) of the depth profile at 100 μm for 31 rocks reported in 21 papers (references are given in Table 1). We have attempted to include in Fig. 5 most of the published data measured in rock crystals; no measurements in glass are included. All data points shown are based on our own fits to published data before authors' corrections for any presumed recent chipping or dust shielding. Errors in track density are

generally about 10% and errors in exponent are 10%–20% depending on the smoothness of the profile. Open circles refer to special samples originally chosen to yield the production profile, with exponents of 1.8–2.5. Most rocks show much shallower profiles, varying over a wide range within the parallelogram marked in Fig. 5.

Model results: Clean rocks

Some results of model calculations for impact-saturated rock surfaces kept continuously clean are shown in Fig. 6 by circular points. The most important
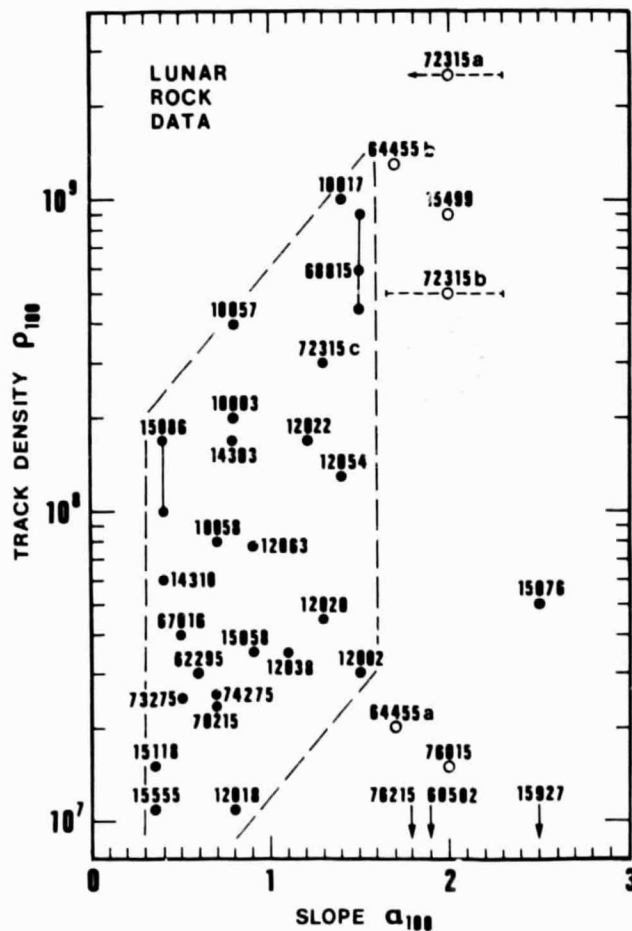

Fig. 5. Measured track density at 100 μm plotted against the negative exponent of the depth profile at 100 μm for 31 rocks reported in 21 papers. References are given in Table 1. Open circles refer to special samples chosen to yield the track production profile.

model parameters are α, the negative exponent of the solar flare track production profile, and ϕ, a meteoroid flux factor equal to the number of impacts per cm^2-10^6 years with central pit diameter greater than 500 μm. The parameter η is a dust accumulation factor which is 0 for clean rocks. The rate $\phi = 5$ refers to the crater production rate in Fig. 3 marked *lunar rock data* and $\phi = 50$ refers to *lunar $\times$ 10*, which fits the satellite data better. The label Model I refers to the shape of these two crater production curves. Exponent $\alpha = 1.8$ represents the shallowest track production profile suggested by lunar data (curve *b* in Fig. 4, from Blanford *et al.*, 1975) while $\alpha = 2.2$ is a more representative model. The dashed parallelogram outlines the normal rock data in Fig. 5. The "error bars" show the total spread obtained in several trial computer runs for a given set of parameter values and represents the variation expected for clean rocks. The dotted arrows connect models of increasing meteoroid flux.

Figure 6 shows that only by taking the shallowest possible track production profile, $\alpha = 1.8$, and a high impact rate can we obtain results falling just within the range of normal rock data, and even this case does not explain most of the impact-saturated rock surfaces measured. Models with $\alpha \geq 2$ lie outside the data range. All clean rock models are found to have the following properties.

Most of the erosion by microcratering is due to the formation of pits larger than about 100 μm diameter. As a result, microcratering can produce enough mass wastage to explain the track profiles at depths $\gtrsim 1$ mm, but does not yield appreciable erosion on a finer size scale. We find that this effect is caused by two independent conditions, either one of which is sufficient to reduce the effect of erosion on the track profile shape at depths ≤ 100 μm. These are: 1) the bend-over in crater production below about 100 μm pit diameter (Fig. 3), and 2) the tendency of pits smaller than ~ 10 μm diameter to lack full spall zones. The occasional removal of large chips of $\gtrsim 100$ μm size temporarily flattens that track profile, but in the absence of fine-scale erosion the profile relatively quickly regains nearly the production slope at 100 μm, with a smooth transition to an erosion-shaped profile at depths greater than 100 μm. The occurrence of a recent, large chip is too rare an event to explain the abundance of shallow track profiles observed (Fig. 5), especially in view of the fact that track workers generally attempt to measure the steepest track profile on each sample. During most of a computer simulation run the calculated track profile has an exponent at 100 μm depth, α_{100}, of 0–0.5 unit less than that of the track production profile, instead of the 1 unit less predicted for fine-scale erosion equilibrium. Increasing the cratering rate causes a decrease in track density as expected and also a slight decrease in exponent because the profile has less time to recover between chipping events.

Model results: Dusty rocks

In order to produce the kind of universal degradation shown in Fig. 5 we need a mechanism which continually changes the exposure depth in increments of much less than 100 μm. Impacts apparently do not do this efficiently, but fine

Table 1. Track profile measurements in lunar rock crystals.

Rock	Reference	Remarks
10003	Price and O'Sullivan (1970)	
10017	Fleischer et al. (1970)	
10057	Crozaz et al. (1971)	Average of different regions
10058	Crozaz et al. (1970)	Extrapolated from 30 μm to 100 μm
12002	Bhandari et al. (1971)	
12018	Bhandari et al. (1971)	
12020	Bhandari et al. (1971)	
12022	Barber et al. (1971)	
12038	Bhandari et al. (1971)	
12054	Morrison and Zinner (1977)	Feldspar crystal in glass coating
12063	Crozaz et al. (1971)	
14303	Bhandari et al. (1972)	
14310	Crozaz et al. (1972)	
15058	Bhandari et al. (1973)	
15076	Schneider et al. (1972)	
15086	Goswami et al. (1976b)	
15118	Bhandari et al. (1973)	
15499	Hutcheon et al. (1972)	Bottom of a surface vug
15555	Bhandari et al. (1973)	
15927	Schneider et al. (1972)	
60502	Storzer et al. (1973)	
62295	Bhandari et al. (1973)	
64455(a)	Blanford et al. (1975)	Quench crystal, raw data
64455(b)	Blanford et al. (1975)	Quench crystal, normalized
67016	Bhandari et al. (1973)	
68815	Dust and Crozaz (1977)	Three locations measured
70215	Goswami and Lal (1974)	
72315(a)	Hutcheon et al. (1974)	Inside crevice, uncorrected
72315(b)	Hutcheon et al. (1974)	Fresh crystal inside crevice
72315(c)	Hutcheon et al. (1974)	Outside of boulder
73275	Goswami and Lal (1974)	
74275	Goswami and Lal (1974)	
76015	Crozaz et al. (1974)	Inside narrow crevice
76215	Morrison and Zinner (1977)	

dust accumulation can. Lunar rocks reside in a dusty environment which generally experiences a fine-scale accumulation rate of about 4 mm/10^6 years (e.g., Comstock, 1977a). Assuming that only some fine fraction of this will stick, however loosely, to rock surfaces, we may expect an accumulation on rocks of 0.3 to 3 mm/10^6 years. This accumulation would be modulated and occasionally cleaned off by impacts. To evaluate this effect we included in the model a steady accumulation of fine dust described by an efficiency parameter η, defined to be
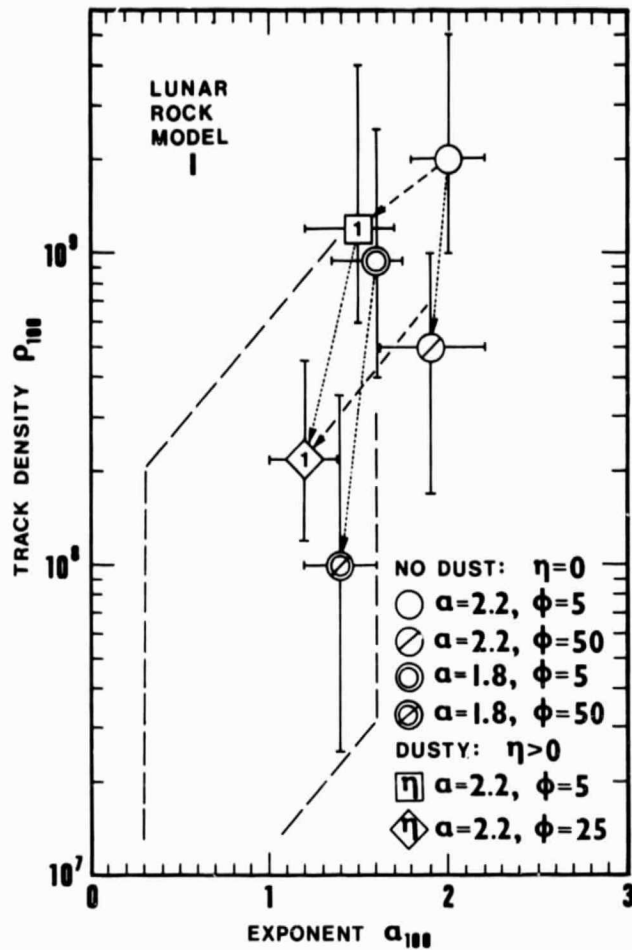
Fig. 6. Calculated track density at 100 μm plotted against the negative exponent of the depth profile at 100 μm for models of impact-saturated rock surfaces which are assumed to be continuously clean (no dust), along with two dusty rock models. η is a dust accumulation rate parameter defined in the text. α is the track production profile exponent. ϕ is the number of impact pits per cm^2-10^6 years with pit diameter >500 μm. The parallelogram encloses the normal rock data in Fig. 5. Dashed arrows show the effect of adding dust accumulation and dotted arrows show the effect of increasing the meteoroid flux level.

the rate of dust accumulation divided by the rate of removal (erosion) due to impacts with central pits of less than 4 mm diameter.

For $\eta = 1$ we find that the dust is kept well in check by impact cleaning, yielding intermittent, variable coverings less than 100 μm thick on a flat surface. Two typical examples of this case are shown in Fig. 6, by the square for a dust accumulation rate of 0.16 mm/10^6 years, and by the diamond for a 10-

times-higher impact rate and a dust accumulation rate of 1.5 mm/10[6] years. The
dashed arrows indicate the effect of adding even a relatively small amount of dust
with other parameters constant.

If the rock surfaces are indeed usually covered with a dust layer, then this
layer will also partially shield the surface from micrometeoroids resulting in a
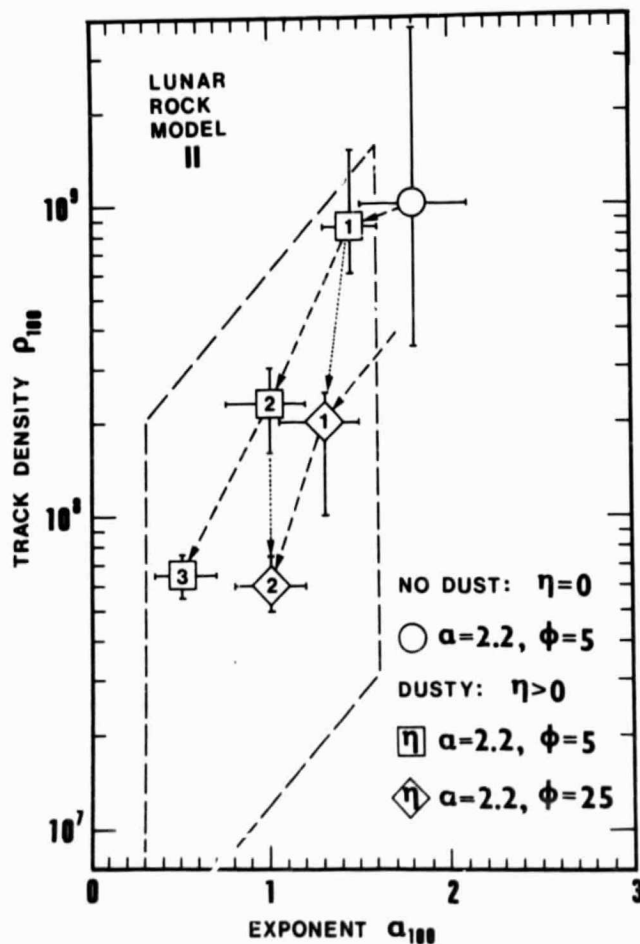reduction in the apparent rate of smaller impacts. This reduction, or shielding

Fig. 7. Calculated track density at 100 μm plotted against the negative exponent of the
depth profile at 100 μm for self-consistent models of rock surfaces subjected to a steady
accumulation of dust. η is a dust accumulation rate parameter defined in the text. The
parallelogram encloses the normal rock data in Fig. 5. Dashed arrows show the effect of
increasing the dust accumulation efficiency with fixed impact rate and dotted arrows
show the effect of increasing impact and dust accumulation rates proportionally.

factor, should be dependent on crater size for ~10 μm to ~1 mm diameter pits, and dependent on the actual dust-free exposure time for micron and submicron pits. Tracks profiles alone do not help much in determining this factor; a more detailed analysis of the dust layer, the cratering process in a thin dust layer, and the effect of surface condition is needed. A self-consistent model will therefore involve some higher micrometeoroid flux. This could eliminate any need to invoke a time-dependent meteoroid flux as has been suggested by satellite measurements (Fig. 3); but the reader is reminded that there are serious difficulties in interpreting the satellite data (Hörz *et al.*, 1975), and it is not clear how much disagreement there actually is between the lunar and satellite micrometeoroid flux determinations. Finally, since dust accumulation is in competition with removal by impacts, the strongest test case for the dust hypothesis will assume the steepest plausible crater production size distribution.

In order to investigate these effects we have also tried in the model the steeper crater production curves in Fig. 3 marked *a*, *b*, and *c*, which we refer to as Model II. Curve *a* has the form $N(>D) = 8.3 \times 10^{-4}D^{-3}$, where D is the pit diameter in cm; curve *b* is 5 times higher; and curve *c* is 10 times higher. Considering the satellite data in Fig. 3 it is likely that the true crater production curve does have an inflection at 10–100 μm pit diameter, not primarily due to shielding. In fact the model results show that we may tailor curves *a*, *b*, and *c* in Fig. 3 to bend over below 50–100 μm, in order to follow the satellite data, without strongly altering calculated track profiles at 100 μm depth, with or without dust. For example curves *b* and *c* give results similar to the *lunar ×10* production curve.

Figure 7 shows some results for models assuming crater production curves *a* ($\phi = 5$) or *b* ($\phi = 25$), with or without a bend-over below 50–100 μm. These results may be more appropriate for dusty rocks than those shown in Fig. 6. To emphasize the effect of dust we have included in Fig. 7 a computer run with $\eta = 0$ (clean rock) shown by the circle; this point also shows that the bend-over in crater production is not the only factor preventing clean rock models from matching observed track profiles at 100 μm depth. The dust accumulation rates, before modulation by impacts, for the models shown in Fig. 7 are as follows. With $\phi = 5$: 0.3, 0.6, and 0.9 mm/10^6 years for $\eta = 1$, 2, and 3, respectively; with $\phi = 25$: 1.5 and 3.0 mm/10^6 years for $\eta = 1$ and 2, respectively.

As before, $\eta = 1$ yields dust layers only up to ~100 μm thick. For higher η the dust begins to get the upper hand; for $\eta = 3$ only the large impacts are efficient in cleaning dust off, and the covering can build to 1 mm on a flat surface. The efficiency with which dust will stick to a rock surface should depend on the orientation, roughness, and other surface conditions, so the rate of dust accumulation will vary over a rock and from rock to rock, thus producing a wide variation in track profiles as is observed. Rocks in the lower part of the parallelogram have clearly had a history of partial burial.

We have included in the present dust model only the effects of impacts on removing accumulated dust. Electrostatic effects also may play an important role in both the deposition and the removal of dust from rocks (see Pelizzari and Criswell, 1978, and references therein).

3. MODEL DERIVATION OF TRACK PARAMETERS IN LUNAR SOIL LAYERS

Track parameters

In order to usefully characterize the great amount of particle track density data obtained from many soil samples we need to employ statistical track parameters which are both convenient to measure and readily interpretable. The most widely used parameters are ρ_{min}, the minimum track density; ρ_q, quartile density; ρ_{med}, median density; N_H/N, the fraction of grains with either $\rho > 10^8$ cm^{-2} or a track density gradient; and the fraction with $\rho > 10^8$ cm^{-2} which we denote N_8/N. ρ_{min} clearly can be used to estimate the maximum exposure time for units deposited as a single layer and buried all at once (Crozaz *et al.*, 1970). On the other hand, much of the soil appears to have been deposited and buried in finer increments of less than about 1 mm, so a single irradiation depth cannot be identified and a fine-scale burial rate together with surface mixing have more significance than a single exposure time of a static layer (Comstock, 1977a). The possibility of multiple episodes near the surface (pre-irradiation) also complicates the interpretation of track parameters (see Gault *et al.*, 1974 for further discussion).

In order to interpret the track parameters more quantitatively in such cases we have derived them with a Monte-Carlo soil model developed by Comstock (1976, 1977a) and used there to interpret track density gradient parameters. The model characterizes soil layers in terms of a fine-scale surface burial rate L, generally about 4 mm/10^6 years, and the number of surface exposure episodes, N_{SEE}, during which the soil has been exposed to solar flare particles within 1 mm of the surface while subjected to micrometeoroid gardening. $N_{SEE} = 0$ refers to soil deposited in a layer much thicker than 1 mm and never exposed to solar flare particles; for these cases the track parameters depend simply on layer thickness. The severe depth dependence of impact gardening can result in the upper part of a soil unit, the miniregolith, having $N_{SEE} > 1$ while the lower part has $N_{SEE} = 0$. Hence pre-irradiated soil samples and disturbed units may be complex mixtures of these "pure" models, no longer characterized by a single value of N_{SEE} or L.

Soil model

Our model treats individually all events with a depth greater than 100 μm whether layering or excavation, which roughly balance. The net accumulation of material on a scale smaller than 100 μm is treated as a continuous process which will depend on local topography and hence may vary from sample to sample. Hence a range of values is tried for the fine-scale burial rate L from 1 to 10 mm/10^6 years. A detailed description of this model is given by Comstock (1977a). The cratering event rate distribution used in the model is given by Comstock (1977a, Fig. 6) and is based primarily on the meteoroid flux used by Gault *et al.* (1974). The track production rate used is given by Comstock (1977a, Fig. 8) and is based on the revised energy spectra given by Walker and Yuhas (1973) and by Hutcheon *et al.* (1974). No time variations in either micrometeor-

oid flux or charged particle flux are assumed. The present model also includes the contribution of galactic cosmic rays as a layer is continuously buried through several centimeters depth. This contribution will vary if a layer is catastrophically buried or re-exposed by relatively larger events; in any case, it is generally much less than the solar flare particle track accumulation, except for soil never exposed within 1 mm of the surface.

The history of emplacement of a particular sample near the surface is governed by one (for fresh soil) or a few relatively rare, large events, hence we expect any distribution and mixture of N_{SEE} values from 0 for immature samples to <50 for mature samples since a purely statistical model can place no strong constraints on what sequence of characteristics we might expect to find in a particular series of
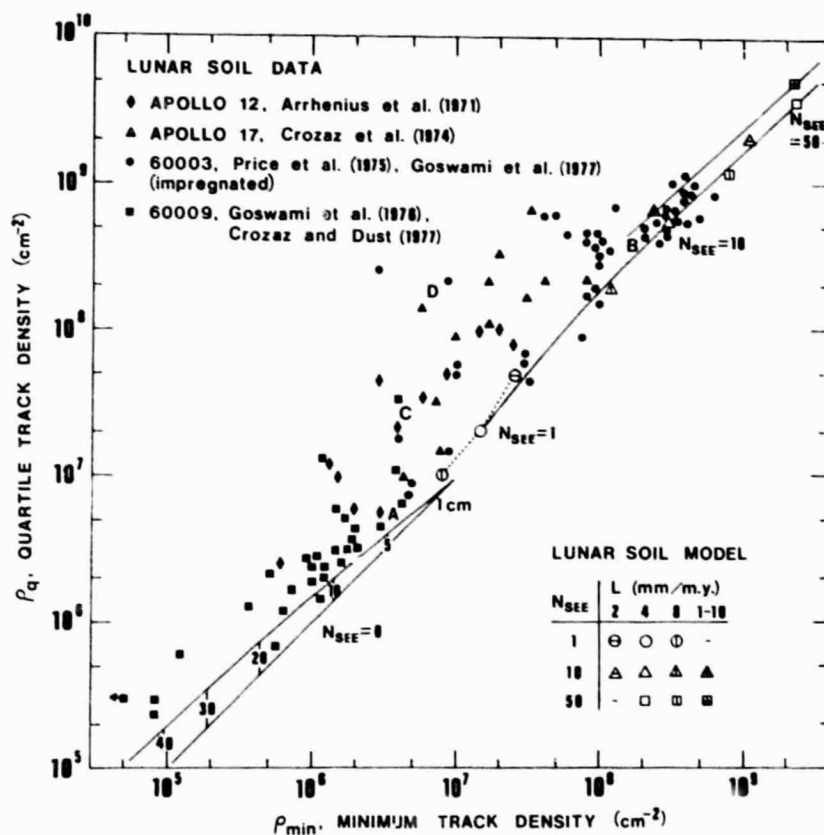

Fig. 8. Results of soil model calculations for minimum and quartile track densities plotted together with selected soil data. Pure models described by single values of surface burial rate L and number of surface exposure episodes N_{SEE} lie near the solid lines, mixtures of these lie off the line. For example, component soils at A and B will have mixtures along line A-C-D. N_{SEE} = 0 means no solar flare particle exposure, for units of the thickness shown, in cm.

soil samples. Our approach therefore is not to generate possible sequences of simulated soil layers, but to use N_{SEE} as a meaningful track maturation parameter derived with the help of the model from measured track parameters such as ρ_{min}, ρ_q, ρ_{med}, and N_H/N.

Results

The results of these calculations are most usefully presented as correlation plots between measured parameters. Figure 8 shows a plot of ρ_q vs. ρ_{min} calculated by the soil model for the various parameter values indicated, along with some soil data selected to show the wide variation observed among real soil layers. The model points are based on 100 simulated grains of 100 μm diameter; data points
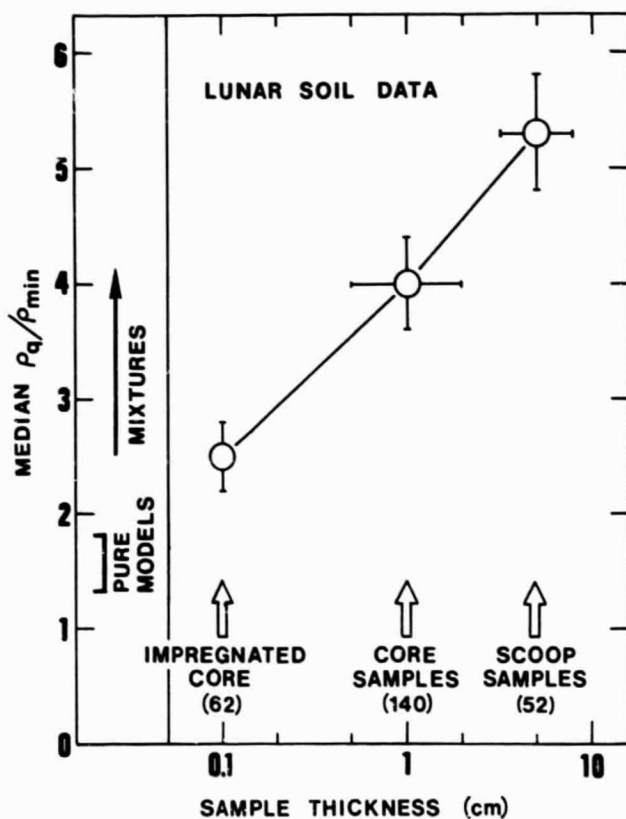

Fig. 9. A plot of the median values of the measured ratios ρ_q/ρ_{min} for most published soil data collected according to sample type, corresponding roughly to thickness sampled. The number of samples in each category is given in parentheses. The range of ρ_q/ρ_{min} values calculated for pure models and for mixtures are indicated for comparison.

are generally based on about 25 measured grains of similar size. Pure models, those represented by single values of L and N_{SEE}, all lie near the solid lines in Fig. 8. The two models marked $L = 1-10$ mm/10^6 years incorporated a different, random L value for each surface exposure episode simulated. The dart marked $N_{SEE} = 0$ refers to units of the thickness indicated, in cm, and is calculated for a representative burial rate of $L = 4$ mm/10^6 years; lower or higher values of L will slide the dart proportionally up or down the diagonal, respectively. The width of the dart represents the difference between sampling the whole thick unit or only the bottom part of it.

In general a soil sample will be some mixture of components with different N_{SEE} values, or maturity, and will lie on a mixing line with ρ_{min} similar to that of the least-irradiated component measured and ρ_q less than that of the most-irradiated component. For example, when a sample with no solar flare exposure from a unit a few cm thick, indicated by the letter A in Fig. 8, is mixed with a highly irradiated sample at point B the mixture will lie somewhere along the line A-C-D and have a much broader distribution of track densities. The data shown
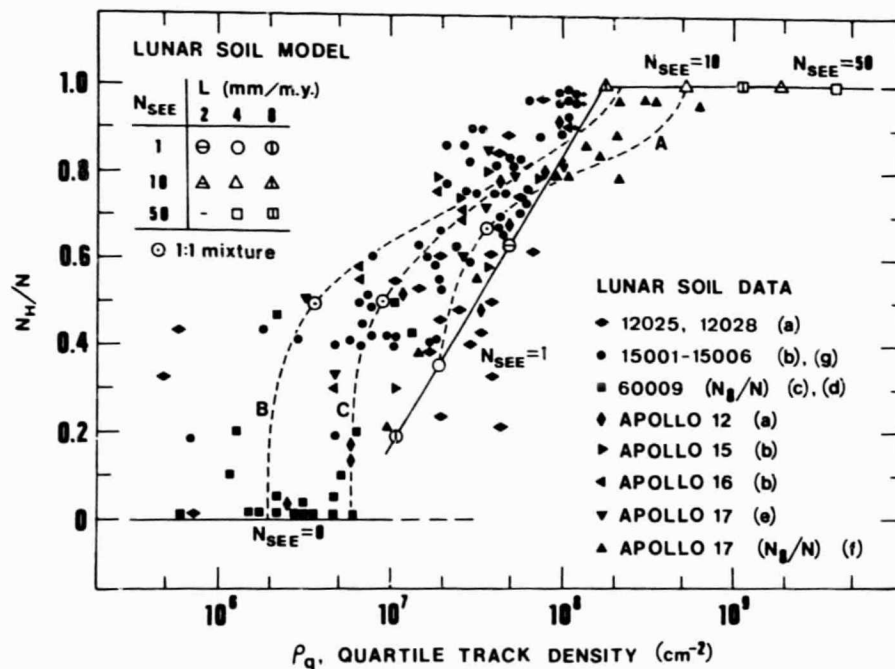

Fig. 10. Results of the soil model calculations for the correlation between the track parameters N_H/N and ρ_q plotted together with soil data. Pure models lie along the solid lines; three examples of mixing lines between two pure model components are shown by dashed lines. (a) Arrhenius *et al.* (1971), (b) Bhandari *et al.* (1973), (c) Goswami *et al.* (1976a), (d) Crozaz and Dust (1977), (e) Goswami and Lal (1974), (f) Crozaz *et al.* (1974), (g) Goswami and Lal (1977).

in Fig. 8 imply that material from thick units are less involved in mixtures.

Individual soil samples are well characterized by their position on a ρ_q vs. ρ_{min} plot, and it is clear which samples are more homogeneous and which are mixtures, and approximately what the components are. Only a fraction of the available data is shown in Fig. 8; we find that each sample site tends to have a particular signature on a ρ_q vs. ρ_{min} plot, so we cannot define an average soil. Plotting ρ_q vs. ρ_{min} emphasizes the lightly-irradiated component of a mixture; we could also plot ρ_{med} vs. ρ_{min} which brings out the more irradiated components.

One interesting result complicates the interpretation of soil samples. When many different samples are plotted on a ρ_q vs. ρ_{min} diagram we find that scoop samples tend to lie further from the pure model line and millimeter-by-millimeter samples from impregnated cores tend to lie the closest to this line. This effect is illustrated best in Fig. 9, where we have separated all available soil data into three categories according to the type of sample, corresponding roughly to thickness sampled: impregnated cores (1 mm intervals), regular core samples (0.5–2 cm intervals), and scoop samples ($\sim$5 cm thick) and determined for each category the median value of the ratios ρ_q/ρ_{min} obtained from individual samples. The ratios ρ_q/ρ_{min} calculated for pure models and for mixtures are also indicated for comparison. The range of ρ_q/ρ_{min} for pure models is very small, $1.2 \lesssim \rho_q/\rho_{min} \lesssim 2.0$, because ρ_q/ρ_{min} is nearly independent of L and N_{SEE}. It is also independent of time variations in the track production rate and nearly independent of time variations in the impact rate. ρ_q/ρ_{min} is strongly increased only by mixing. The trend evident in Fig. 9 suggests that the sampling procedure itself has artificially mixed thin layers with different surface exposure histories, implying the general existence of microstratigraphy on a size scale similar to that of the surface maturation zone or miniregolith and with track properties similar to those derived for miniregoliths.

Goswami and Lal (1974) introduced the N_H/N vs. ρ_q diagram in an attempt to isolate evidence for a time variation in the micrometeoroid flux. The result of our calculations deriving N_H/N vs. ρ_q are shown in Fig. 10. Pure models are connected by the solid line and three examples of mixing lines between pure models are shown. This type of plot is somewhat less useful than ρ_q vs. ρ_{min} for two reasons. First, the definition of N_H/N forces the data and models to follow a general trend similar to that shown because the region with both $\rho_q > 10^8$ cm^{-2} and $N_H/N < 0.75$ is forbidden. Secondly, the mixing lines connecting pure models tend to lie close to the pure model line so it is difficult to distinguish mixtures unless one component has had no solar flare irradiation, in which case N_H/N is a good indicator of a small admixture of highly irradiated soil. The spread of data in Fig. 10 is consistent with calculated models and mixing lines, without the need to invoke time variations. Time variations are not ruled out. However, their record is obscured by the complicating effects of mixing.

4. CONCLUSIONS

Our analysis of solar flare particle track profiles in lunar rocks indicates that

erosion mechanisms alone are insufficient to account for the observed profiles at depths less than a few hundred microns. A Monte-Carlo model which includes the steady accumulation of dust at rates of 0.3 to 3 mm/10^6 years, depending on sticking efficiency, readily explains the magnitude, slope, and wide variation of observed track profiles. Variable dust layers with thicknesses from 100 μm to 1 mm are expected, depending on sticking efficiency and impact rates. The details of this dust layer and its effects on rock surface exposure need to be studied further; the dust cover is capable of drastically reducing the surface exposure time.

Using a Monte-Carlo soil model we have derived common statistical particle track parameters such as ρ_{min}, ρ_q, and N_H/N in terms of physical parameters characterizing the exposure of soil grains in surface mixing and maturation zones, a form of miniregolith, a few millimeters thick. A plot of ρ_q vs. ρ_{min} is very useful for determining the degree of mixing and surface exposure for individual soil samples; the ratio ρ_q/ρ_{min} is a good indicator of mixing. It is concluded that remnants of ancient surface miniregoliths are common in lunar soil, and often have been artificially mixed together upon sampling.

These results are important for the general study of miniregoliths on space-exposed surfaces, including the correlations among the various maturation indices and the evolution of asteroidal and meteorite parent body surfaces.

REFERENCES

Arrhenius G., Liang S , Macdougall D., Wilkening L., Bhandari N., Bhat S., Lal D., Rajagopalan G., Tamhane A. S. and Venkatavaradan V. S. (1971) The exposure history of the Apollo 12 regolith. *Proc. Lunar Sci. Conf. 2nd*, p. 2583–2598.

Barber D. J., Cowsik R., Hutcheon I. D., Price P. B. and Rajan R. S. (1971) Solar flares, the lunar surface, and gas-rich meteorites. *Proc. Lunar Sci. Conf. 2nd*, p. 2705–2714.

Bhandari N., Bhat S., Lal D., Rajagopalan G., Tamhane A. S. and Venkatavaradan V. S. (1971) High resolution time averaged (millions of years) energy spectrum and chemical composition of iron-group cosmic ray nuclei at 1 A.U. based on fossil tracks in Apollo samples. *Proc. Lunar Sci. Conf. 2nd*, p. 2611–2619.

Bhandari N., Goswami J. N., Gupta S. K., Lal D., Tamhane A. S. and Venkatavaradan V. S. (1972) Collision controlled radiation history of the lunar regolith. *P··c. Lunar Sci. Conf. 3rd*, p. 2811–2829.

Bhandari N., Goswami J. N. and Lal D. (1973) Surface irradiation and evolution of the lunar regolith. *Proc. Lunar Sci. Conf. 4th*, p. 2275–2290.

Blanford G. E., Fruland R. M. and Morrison D. A. (1975) Long-term differential energy spectrum for solar-flare iron-group particles. *Proc. Lunar Sci. Conf. 6th*, p. 3557–3576.

Brownlee D. E., Hörz F., Hartung J. B. and Gault D. E. (1975) Density, chemistry, and size distribution of interplanetary dust. *Proc. Lunar Sci. Conf. 6th*, p. 3409–3416.

Comstock G. M. (1976) Particle tracks and lunar soil exposure history (abstract). In *Lunar Science VII*, p. 169–171. The Lunar Science Institute, Houston.

Comstock G. M. (1977a) On deciphering the particle track record of lunar regolith history. *J. Geophys. Res.* **82**, 357–367.

Comstock G. M. (1977b) New techniques for simulation of lunar surface processes (abstract). In *Lunar Science VIII*, p. 202–204. The Lunar Science Institute, Houston.

Criswell D. R. (1972) Lunar dust motion. *Proc. Lunar Sci. Conf. 3rd*, p. 2671–2680.

Crozaz G., Drozd R., Hohenberg C. M., Hoyt H. P., Jr., Ragan D., Walker R. M. and Yuhas D. (1972) Solar flare and galactic cosmic ray studies of Apollo 14 and 15 samples. *Proc. Lunar Sci. Conf. 3rd*, p. 2917–2931.

Crozaz G., Drozd R., Hohenberg C., Morgan C., Ralston C., Walker R. and Yuhas D. (1974) Lunar surface dynamics: Some general conclusions and new results from Apollo 16 and 17. *Proc. Lunar Sci. Conf. 5th*, p. 2475–2499.

Crozaz G. and Dust S. (1977) Irradiation history of lunar cores and the development of the regolith. *Proc. Lunar Sci. Conf. 8th*, p. 3001–3016.

Crozaz G., Haack U., Hair M., Maurette M., Walker R. M. and Woolum D. (1970) Nuclear track studies of ancient solar radiations and dynamic lunar surface processes. *Proc. Apollo 11 Lunar Sci. Conf.*, p. 2051–2080.

Crozaz G., Walker R. and Woolum D. (1971) Nuclear track studies of dynamic surface processes on the moon and the constancy of solar activity. *Proc. Lunar Sci. Conf. 2nd*, p. 2543–2558.

Duraud J. P., Langevin Y., Maurette M., Comstock G. M. and Burlingame A. L. (1975) The simulated depth history of dust grains in the lunar regolith. *Proc. Lunar Sci. Conf. 6th*, p. 2397–2415.

Dust S. and Crozaz G. (1977) 68815 revisited. *Proc. Lunar Sci. Conf. 8th*, p. 2315–2319.

Fleischer R. L., Haines E. L., Hart H. R., Jr., Woods R. T. and Comstock G. M. (1970) The particle track record of the Sea of Tranquility. *Proc. Apollo 11 Lunar Sci. Conf.*, p. 2103–2120.

Fleischer R. L., Hart H. R., Jr. and Giard W. R. (1974) Surface history of lunar soil and soil columns. *Geochim. Cosmochim. Acta* 38, 365–380.

Fleischer R. L., Price P. B. and Walker R. M. (1975) Ancient energetic particles in space. In *Nuclear Tracks in Solids*, p. 307–431. University of California Press, Berkeley, Calif.

Gault D. E., Hörz F., Brownlee D. E. and Hartung J. B. (1974) Mixing of the lunar regolith. *Proc. Lunar Sci. Conf. 5th*, p. 2365–2386.

Goswami J. N., Borg J., Langevin Y., Maurette M. and Price P. B. (1977) Microstratification in Apollo 15 and 16 core tubes: Implications to regolith dynamics (abstract). In *Lunar Science VIII*, p. 365–367. The Lunar Science Institute, Houston.

Goswami J. N., Braddy D. and Price P. B. (1976a) Microstratigraphy of the lunar regolith and compaction ages of lunar breccias. *Proc. Lunar Sci. Conf. 7th*, p. 55–74.

Goswami J. N., Hutcheon I. D. and Macdougall J. D. (1976b) Particle track and microcrater records in lunar samples and meteorites. *Proc. Lunar Sci. Conf. 7th*, p. 543–562.

Goswami J. N. and Lal D. (1974) Cosmic ray irradiation pattern at the Apollo 17 site: Implications to lunar regolith dynamics. *Proc. Lunar Sci. Conf. 5th*, p. 2643–2662.

Goswami J. N. and Lal D. (1977) Particle track correlation studies in lunar soils: Possible long-term periodic fluctuations in ancient meteoritic flux at 1 A.U. *Proc. Lunar Sci. Conf. 8th*, p. 813–824.

Hartung J. B., Hodges F. and Hörz F., Storzer D. (1975) Microcrater investigations on lunar rock 12002. *Proc. Lunar Sci. Conf. 6th*, p. 3351–3371.

Hartung J. B., Hörz F., Aitken F. K., Gault D. E. and Brownlee D. E. (1973) The development of microcrater populations on lunar rocks. *Proc. Lunar Sci. Conf. 4th*, p. 3213–3234.

Hörz F., Brownlee D. E., Fechtig H., Hartung J. B., Morrison D. A., Neukum G., Schneider E., Vedder J. F. and Gault D. E. (1975) Lunar microcraters: Implications for the micrometeoroid complex. *Planet. Space Sci.* 23, 151–172.

Hörz F., Schneider E. and Hill R. E. (1974) Micrometeoroid abrasion of lunar rocks: A Monte-Carlo simulation. *Proc. Lunar Sci. Conf. 5th*, p. 2397–2412.

Hutcheon I. D., Braddy D., Phakey P. P. and Price P. B. (1972) Study of solar flares, cosmic dust and lunar erosion with vesicular basalts (abstract). In *The Apollo 15 Lunar Samples* (J. W. Chamberlain and C. Watkins, eds.), p. 412–414. The Lunar Science Institute, Houston.

Hutcheon I. D., Macdougall J. D. and Price P. B. (1974) Improved determination of the long-term average Fe spectrum from ~1 to ~460 MeV/amu. *Proc. Lunar Sci. Conf. 5th*, p. 2561–2576.

McDonnell J. A. M. (1977) Accretionary particles: Production and equilibrium of 12054. *Proc. Lunar Sci. Conf. 8th*, p. 3835–3857.

McDonnell J. A. M., Ashworth D. G., Flavill R. P. and Jennison R. C. (1972) Simulated microscale erosion on the lunar surface by hypervelocity impact, solar wind sputtering, and thermal cycling. *Proc. Lunar Sci. Conf. 3rd*, p. 2755–2765.

McDonnell J. A. M. and Carey W. C. (1975) Solar-wind sputter erosion of microcrater populations on the lunar surface. *Proc. Lunar Sci. Conf. 6th*, p. 3391–3402.

Morrison D. and Zinner E. (1977) Microcraters and solar cosmic ray tracks (abstract). In *Lunar Science VIII*, p. 691–693. The Lunar Science Institute, Houston.

Pelizzari M. A. and Criswell D. R. (1978) Lunar dust transport by photoelectric charging (abstract). In *Lunar and Planetary Science IX*, p. 876–878. Lunar and Planetary Institute, Houston.

Price P. B., Hutcheon I. D., Braddy D. and Macdougall D. (1975) Track studies bearing on solar-system regoliths. *Proc. Lunar Sci. Conf. 6th*, p. 3449–3469.

Price P. B. and O'Sullivan D. (1970) Lunar erosion rate and solar flare paleontology. *Proc. Apollo 11 Lunar Sci. Conf.*, p. 2351–2359.

Schneider E., Storzer D. and Fechtig H. (1972) Exposure ages of Apollo 15 samples by means of microcrater statistics and solar flare particle tracks (abstract). In *The Apollo 15 Lunar Samples* (J. W. Chamberlain and C. Watkins, eds.), p. 415–419. The Lunar Science Institute, Houston.

Seitz M. G. and Wittels M. C. (1971) A limit on the radiation erosion in lunar surface material. *Earth Planet. Sci. Lett.* **10**, 268–270.

Storzer D., Poupeau G. and Krätschmer W. (1973) Track-exposure and formation ages of some lunar samples. *Proc. Lunar Sci. Conf. 4th*, p. 2363–2377.

Walker R. and Yuhas D. (1973) Cosmic ray track production rates in lunar materials. *Proc. Lunar Sci. Conf. 4th*, p. 2379–2389.

Zook H., Hartung J. B. and Hauser E. (1978) Loosely bound dust, impact pits, and accreta on lunar rock 12054,54 (abstract). In *Lunar and Planetary Science IX*, p. 1300–1302. Lunar and Planetary Institute, Houston.